UNIVERSITY OF CALIFORNIA
RIVERSIDE

Development in *Aulacopleura koninckii* - Glimpses into the Evolution of Body Organization in an Early Arthropod Clade

A Thesis submitted in partial satisfaction
of the requirements for the degree of

Master of Science

in

Geological Sciences

by

Paul Hong

December 2011

Thesis Committee:

Dr. Nigel C. Hughes, Chairperson
Dr. Mary L. Droser
Dr. Gordon D. Love

The Thesis of Paul Hong is approved:

_____

_____

_____
Committee Chairperson

University of California, Riverside

ABSTRACT OF THE THESIS

Development in *Aulacopleura koninckii*
- Glimpses into the Evolution of Body Organization in an Early Arthropod Clade

by

Paul Hong

Master of Science, Graduate Program in Geological Sciences
University of California, Riverside, December 2011
Dr. Nigel C. Hughes, Chairperson

A concentration of well preserved, articulated juvenile and mature exoskeletons of the Czech middle Silurian trilobite *Aulacopleura koninckii* provides an unparalleled opportunity to explore the nature of exoskeletal growth and morphological variation during trilobite development. A new dataset selected via a comprehensive survey of the highest quality specimens offers improved resolution of original morphology by all measures considered. It confirms that meraspid size increase was exponential and the meraspid growth rate per instar was strikingly constant. The degree of variation in both size and shape among later meraspid instars was remarkably constant, and suggests that an active process channeled the meraspid development of both these attributes. The degree of precision of the growth control is remarkable given this species' well-known variance in holaspid trunk segment number. Size-related changes in the

shape of the dorsal exoskeleton and of the segment-invariant cephalon were detected in the meraspid stage, but in the holaspid phase marked allometry was detected only in the trunk region, with the pygidium showing notable expansion in relative size. Meraspid cranidial allometry was subtle, with significant changes in instar form detectable only after several molts. Analyses suggest that this synarthromeric trilobite developed progressively without sharp transition throughout meraspid and holaspid ontogeny, except for the synchronous cessation of trunk segment appearance and release at the onset of the holaspid phase. We suggest that the remarkably tight control of the development of sclerite size and shape, and the gradual, “track-like” ontogeny of *A*. *koninckii* may have resulted from development in conditions of reduced oxygen availability in which physiological viability operated within narrow morphological limits.

Table of Contents

Introduction

Arthropod bodies are built from sets of serially repeated structural units called segments. Variation in the manner of segment expression, integration of segment boundaries among tissues, the total number of segments, and regionalization of segment form underpins much of the diversity of the phylum. Exploration of the developmental mechanisms responsible for the specification of segments and the differences among them is currently a major area of research in developmental and evolutionary biology (e.g. Akam, 2000; Damen and Tautz, 1999; Janssen et al., 2004; Minelli and Fusco, 2004; Patel, 1994; Pourquie, 2003; Damen et al., 2005; Liu and Kaufman, 2005). Recent symposia and thematic volumes have sought to foster cross disciplinary approaches to segmentation that include fossil-based perspectives (Hughes and Jacobs, 2005). The fossil record provides an unique viewpoint on the early evolution of metazoan segmentation (Jacobs et al., 2005) because some fossil groups, and most particularly arthropods, record a wealth of data on the sequential development of segments. Studies of ancient ontogenies can provide insights into the manner in which segments were constructed and modified among euarthropod and crustacean stem groups (Hughes, 2005; Walossek 1993; Waloszek and Maas, 2005), and thus provide an empirical basis for assessing the evolution of segmentation among living and extinct arthropods. Such studies suggest that a major and repeated macroevolutionary trend in arthropod

evolution was increased regionalization and specialization of body segments and their associated appendages (Budd, 2000; Cisne, 1974; Hughes, 2003; Wills et al., 1997). Insights into the ways in which this regionalization arose remain preliminary (Averof and Patel, 1997; Budd, 1999).

There are two major components to this trilobite developmental research. The first is a detailed analysis of trunk segment development in the middle Silurian aulacopleurid trilobite *Aulacopleura koninckii*. This species has proved singularly useful as a model system for exploring the controls upon variation in trunk segment numbers within a single trilobite species (Fusco et al., 2004; Hughes and Chapman, 1995; Hughes et al., 1999). Arrangement of arthropod bodies into sets of similar segments is contingent upon controlling the numbers of segments, because high levels of regionalization occurs in forms with stable numbers of segments (Hughes, 2003). Hence this study will provide insights into both the microevolutionary origins of the changes in segment numbers evident among trilobites (Hughes, 2005), and into the prerequisites for arthropod body regionalization. A series of hypotheses are outlined, and test of these will illuminate the ways in which trunk organization was controlled in *A*. *koninckii*. The study addresses the core question on the mechanism in the arthropod body plan to vary its segment numbers (Carroll et al., 2004, p. 232), and represents a significant opportunity for the burgeoning interface between paleobiology and evolutionary developmental biology.

Variation in thoracic segment numbers in maturity, such as in *A*. *koninckii*, assumes a special significance because although quite common among Cambrian trilobite species (Hughes et al., 1999), mature thoracic segment numbers are generally stable at the family level and higher among derived trilobites (McNamara, 1983). This trend toward stable numbers of segments has been labeled the “the paradigmatic example of developmental entrenchment associated with the Cambrian radiation” (Erwin, 2000). Understanding the basis of this trend is central to understanding evolutionary trends in the regulation of arthropod segmentation. Although *A*. *koninckii* showed plasticity in the determination of its segment numbers, there is strong indication that its growth was precisely controlled (Fusco et al., 2004). Hence the second component of this project is a comparison of the variation in segment numbers in mature *A*. *koninckii* with that belonging to the late Cambrian “ptychopariid” trilobites *Labiostria westropi* and *Wujiajiania sutherlandi*, both phylogenetically much less derived within the clade Trilobita with respect to *A*. *koninckii* (Fortey, 1990; Hughes et al., 1999). This study will explore whether the control of segment numbers and overall shape was similar among all these taxa, providing insights into whether and how development became more tightly regulated among derived trilobite clades (Hughes, 1991, 2005; McNamara, 1983), even those, such as *A*. *koninckii*, that showed intraspecific variation in mature trunk segment numbers.

The thesis compiled here is related to the results on the first major component of the trilobite development research, which is analyzing the growth of a derived, post-Cambrian trilobite *Aulacopleura koninckii* and understanding how it achieved variations in segment numbers. Detailed size and shape changes with the growth of *A. koninckii* is discussed in the thesis, and the results will become the foundation for assessing general developmental plans of the trilobite group.

References

AKAM, M. 2000. Arthropods: developmental diversity within a (super) phylum. Proceedings of the National Academy of Sciences, 97:4438–4441.

AVEROF, M., AND N. H. PATEL. 1997. Crustacean appendage evolution associated with changes in Hox gene expression. Nature, 388:682–686.

BUDD, G. E. 1999. Does evolution in body patterning genes drive morphological change or vice versa? BioEssays, 21:326–332.

BUDD, G. E. 2000. Ecology of nontrilobite arthropods and lobopods in the Cambrian, p. 404–427. *In* A. Y. Zhuravlev and R. Riding (eds.), The Ecology of the Cambrian Radiation. Columbia University Press, New York.

CARROLL, S. B., J. K. GRENIER, AND S. D. WEATHERBEE. 2005. From DNA to Diversity. Molecular genetics and the evolution of animal design. Second Edition. Blackwell Science, Oxford, 257 p.

CISNE, J. L. 1974. Evolution of the world fauna of aquatic free-living arthropods. Evolution, 28:337–366.

DAMEN, W. G. M., R. JANSSEN, AND N. M. PRPIC. 2005. Pair rule gene orthologs in spider segmentation. Evolution and Development, 7:618–628.

DAMEN, W. G. M., AND D. TAUTZ. 1999. Abdominal-B expression in a spider suggests a general role for Abdominal-B in specifying genital structure. Journal of Experimental Zoology (Molecules, Development and Evolution), 285:85–91.

ERWIN, D. H. 2000. Macroevolution is more than repeated rounds of microevolution. Evolution and Development, 2:78–84.

FORTEY, R. A. 1990. Ontogeny, hypostome attachment and trilobite classification. Palaeontology, 33:529–576.

FUSCO, G., N. C. HUGHES, M. WEBSTER, AND A. MINELLI. 2004. Exploring developmental modes in a fossil arthropod: Growth and trunk segmentation of the trilobite *Aulacopleura konincki*. American Naturalist, 163:167–183.

HUGHES, N. C. 1991. Morphological plasticity and genetic flexibility in a Cambrian trilobite. Geology, 19:913–916.

HUGHES, N. C. 2003. Trilobite body patterning and the evolution of arthropod tagmosis. Bioessays, 25:386–395.

HUGHES, N. C. 2005. Trilobite construction: Building a bridge across the micro- and macroevolutionary divide, p. 139–158. *In* D. E. G. Briggs (ed.), Evolving Form and Function: Fossils and Development. Peabody Museum of Natural History, Yale University, New Haven, Connecticut.

HUGHES, N. C., AND R. E. CHAPMAN. 1995. Growth and variation in the Silurian proetide trilobite *Aulacopleura konincki* and its implications for trilobite palaeobiology. Lethaia, 28:333–353.

HUGHES, N. C., AND D. K. JACOBS. 2005. The end of everything: metazoan terminal addition. Evolution and Development, 7:497.

HUGHES, N. C., R. E. CHAPMAN, AND J. M. ADRAIN. 1999. The stability of thoracic segmentation in trilobites: a case study in developmental and ecological constraints. Evolution and Development, 1:24–35.

JACOBS, D. K., N. C. HUGHES, S. T. FITZ-GIBBON, AND C. J. WINCHELL. 2005. Terminal addition, the Cambrian radiation and the Phanerozoic evolution of bilaterian form. Evolution and Development, 7:498–514.

JANSSEN, R., N. M. PRPIC, AND W. G. M. DAMEN. 2004. Gene expression suggests decoupled dorsal and ventral segmentation in the millipede *Glomeris marginata*. Developmental Biology, 268:89–104.

LIU, P. Z., AND T. C. KAUFMAN. 2005. Short and long germ segmentation: unanswered questions in the evolution of a developmental mode. Evolution and Development, 7:629–646.

MCNAMARA, K. J. 1983. Progenesis in trilobites, p. 59–68. *In* D. E. G. Briggs and P. D. Lane (eds.), Trilobites and Other Early Arthropods: Papers in Honour of Professor H. B. Whittington, F.R.S. Special Papers in Palaeontology, 30.

MINELLI, A., AND G. FUSCO. 2004. Evo-devo perspectives on segmentation: model organisms and beyond. Trends in Ecology and Evolution, 19:423–429.

PATEL, N. H. 1994. The evolution of arthropod segmentation: insights from comparisons of gene expression patterns. Development, 1994 Supplement:201–207.

POURQUIE, O. 2003. The segmentation clock. Science, 301:328–330.

WALOSSEK, D. 1993. The Upper Cambrian *Rehbachiella* and the phylogeny of Branchiopoda and Crustacea. Fossils and Strata, 32:1–202.

WALOSZEK, D., AND A. MAAS. 2005. The evolutionary history of crustacean segmentation: a fossil-based perspective. Evolution and Development, 7:515–527.

WILLS, M. A., D. E. G. BRIGGS, AND R. A. FORTEY. 1997. Evolutionary correlates of arthropod tagmosis: scrambled legs, p. 57–65. *In* R. A. Fortey and R. H. Thomas (eds.), Arthropod Relationships. The Systematics Association Special Volume Series, 55.

Chapter 1

The Growth in Size and Shape of the Silurian Trilobite *Aulacopleura koninckii*

Paul S. Hong, Nigel C. Hughes, and H. David Sheets

Introduction

This study concerns the growth pattern of a species that has provided important glimpses into the factors controlling developmental regulation in trilobites, the Middle Silurian trilobite *Aulacopleura koninckii*. Large numbers of articulated exoskeletons covering a broad span of juvenile and mature ontogeny occur in a thin interval of siltstone on Na Cernidlech hill near Lodenice in the Czech Republic. Mature specimens within this assemblage show the greatest degree of intraspecific variation in thoracic segment number known in any hemianamorphically-developing trilobite (see Hughes et al., 1999; Hughes et al., 2006), and the presence of such variability in a Silurian trilobite is remarkable because variation in thoracic segment numbers is generally rare among post-Cambrian trilobite species (Hughes et al., 1999). For all these reasons *A. koninckii* serves as a fossilized “model organism”, in that aspects of its morphological dynamics provide a standard to which other arthropods may be compared. Of particular interest is the attempt to understand how the

unprecedented degree of variation in thoracic segment number seen in *A. koninckii* relates to other aspects of the development of this animal, and what insights might this variation provide into the microevolutionary basis of the macroevolutionary changes in the evolutionary history of these early arthropods. This study documents the construction of the new dataset, evaluates its quality, and uses it to explore variation in the size and shape of the major exoskeletal components of *A. koninckii.* This information is then integrated with an updated systematic description of this taxon. Detailed quantitative analysis of the development of individual trunk segments will be described elsewhere.

The geological setting of *A. koninckii* at the Na Cernidlech site

All the material considered in the quantitative analysis presented below came from a 1.4 meter interval of the Homerian *Aulacopleura* shales that likely accumulated over an interval spanning a few thousand years (Hughes et al. 1999). It was deposited on the flanks of a basaltic volcanic massif as part of an extensional basin associated with the Perunica microcontinent (Storch, 2006; Fatka and Mergl, 2009). The taphonomy of the assemblage as assessed from museum collections has been reviewed in Hughes and Chapman (1995), and a further study based on field observations will be published elsewhere. *Aulacopleura koninckii* occurs in large numbers as articulated, partially articulated, and disarticulated specimens on multiple bedding planes within this

interval. The occasional occurrence of enrolled specimens suggests that individual surfaces were buried by obrution events, but the degree of disarticulation present on bedding plane collections suggests that all surfaces are time-averaged to some extent. Prone specimens apparently include both carcasses and intact exuviae. Mean specimen size can vary markedly between individual bedding planes. On some bed surfaces *A. koninckii* is accompanied by a diverse range of Silurian skeletonized benthos, but others are virtually monospecific assemblages of *A. koninckii.* Large specimens bearing different numbers of thoracic segments occur on individual bedding surfaces and, to the maximum stratigraphic resolution available, all of the 5 mature thoracic segment morphotypes occur together. No morphological variations were observed that could distinguish individuals from one bedding plane from those from any other bedding plane.

Prior research on the development of *A. koninckii*

Barrande (1852) described the meraspid ontogeny of *A. koninckii*, documenting the sequential addition of segments. He also noted that large individuals from the Na Cernidlech site displayed between 18 and 22 thoracic segments. Multivariate analysis of various linear dimensions of 86 specimens of *A. koninckii* (Hughes and Chapman, 1995) suggested some patterns of allometric growth and showed that shape variation remained approximately constant during

growth and that shape change between developmental stages occurred gradually, suggesting a track-like developmental trajectory in which changes were progressive and slow. No correlation was detected between the number of segments in the thorax and in the meraspid or holaspid pygidium. Accordingly, variation in thoracic segment numbers was not evidently compensated for, or explained by, variation in the numbers of pygidial segments.

A Procrustes-based geometric analysis was used to compare of the degree of morphological variability among holaspid *A. koninckii* with that of the holaspids of six other trilobite species present in 1.4 m interval (Hughes et al., 1999). Each of these six other species were invariant in the holaspid number of thoracic segments. When differences in degrees of allometry and sample size were taken into account, each species showed a comparable degree of shape variation species (Hughes et al., 1999; Hughes and Chapman, 2001). This comparability contrasted with the variability in thoracic segment numbers seen in mature *A. koninckii* and suggested a degree of compensation between the number of thoracic segments and the sizes of individual segments in that species. The constant holaspid segment number of the other, co-occurrent trilobite species indicated that variation in mature thoracic segment number in *A. koninckii* was specific to that species, and not due to a variable environmental factor that influenced the segmentation of all trilobite species in a similar way.

Analysis of 391 well-preserved specimens, ranging from forms 1.5mm long with 5 thoracic segments to large holaspids over 24 mm long showed

meraspid growth of *A. koninckii* to be remarkable in two ways (Fusco et al., 2004). Firstly, the growth rate between stages (= intermolt phases = instars) was extremely constant from meraspid stage 5 to 17. This suggests that this portion of meraspid growth conformed to Dyar's rule, a geometric progression typical of the development of many arthropods, but not previously recorded in trilobites over an extended set of molts. Secondly, the degree of size variance within stages remained constant during growth. This indicated that size increase in *A. koninckii* was targeted during this portion of ontogeny, rather than showing an expansion of variance that commonly accompanies growth. This result is important not only as the most ancient example of targeted growth known, but also because it suggests that the size range of meraspid instars of *A. koninckii* was under active control.

The degree of size control in *A. koninckii* suggested that, despite the variation the number of holaspid thoracic segments, growth in this trilobite was tightly coordinated. The variation evident in the numbers of thoracic segments at maturity was thus unlikely to reflect the direct influence of variable environmental conditions: in that case size variance would be expected to be a function of developmental stage. The question of the control of the onset of the mature growth phase was addressed by considering whether the mature number of thoracic segments was determined early in ontogeny, or later in ontogeny at the point of transition to the mature form. An earlier suggestion (Hughes and Chapman 1995) that the mature growth phase of *A. koninckii* was accompanied

by the sporadic release of segments into the thorax was refuted by showing that there was no tendency among demonstrably mature forms for segment rich individuals to become more abundant at the expense of segment poor individuals. This situation presented alternative possibilities for the control of the transition into the mature growth phase. The *Early Determination Hypothesis (EDH)* stated that the number of mature thoracic segments was determined precociously and, therefore, independently from meraspid growth. The *Later Determination Hypothesis (LDH)* stated that the mature number of thoracic segments was determined by the stage at which a certain morpho-physiological condition (a critical state of trait *X*) was reached.

Conformity of the data to these two hypotheses was assessed in two ways. Firstly, observed size frequency distributions were compared with those modeled according to the two hypotheses. A *LDH* model with a critical size threshold, *LDHsize*, predicts a smaller size range and a lower minimum size for the segment rich mature morphotypes than *EDH*. Results show that the observed data conforms to the predicted distribution of the *EDH*, but does not fit well with that of the *LDHsize*. Secondly, the authors considered the hypotheses with respect to the growth of the pygidium. This structure showed a sharp change in growth dynamics at the onset of the segment invariant phase when the appearance of new segments ceased. While both *EDH* and *LDHsize* predicted that the pattern of growth after onset of the segment invariant phase would be similar in both morphs (which analysis confirmed), the *EDH* predicts that forms

with fewer thoracic segments would transition into the segment invariant phase with smaller pygidia than segment rich forms. Again, analysis confirmed congruence of the observed values with the *EDH*.

Exploring developmental control in an extinct clade is a difficult task, and plausible hypotheses need not be mutually exclusive nor exhaustive because many different dynamics could be modeled and additional sources of variation considered. At present the *EDH* is the best-supported hypothesis, and the number of mature thoracic segments was apparently determined precociously with the population was composed of five distinct cohorts that were apparently morphologically identical during meraspid growth. Membership of a particular cohort could be under either hereditary (e.g., genetic) or environmental influence.

Hammer and Harper (2006, p. 148-156) used a dataset modified from that of Hughes and Chapman (1995) to illustrate the application of a variety of morphometric techniques. In doing so they discerned several patterns of size-related shape change and also detected an element of shape variation that was induced by shear stress, which they suggested accounted for a small proportion of the total shape variance.

To date, detailed analyses the growth of *A. koninckii* have focused on information about instar size and conformity to Dyar's law. In this analysis we present the results of an investigation of the development of size and shape. To do this we have constructed a new and highly selective dataset of specimens that reduces taphonomically-induced morphological variance to a minimum. In

particular we describe the meraspid and holaspid ontogeny of *A. koninckii*, particularly with respect to growth allometry and assess whether any marked change in allometric trajectory coincides with changes in other aspects of development. We also assess the instar-related pattern of growth rate in size and shape during meraspid ontogeny.

Specimen preparation, measurement, and individual measurement error

All measured specimens came from museum collections, as the legally protected Na Cernidlech site no longer yields *in situ* specimens. Specimens considered were all prone, and lay parallel to bedding. Most were already fully exposed but some were delicately prepared with a pin to expose hidden areas. The fossils were then coated with ammonium chloride sublimate and photographed directly with a Nikon D100 digital camera and macrolens, through a Nikon SMZ-U stereomicroscope with a Nikon CoolPix995 digital camera and with a Leica MZ16 stereomicroscope with a Leica DFC420 digital camera. The resulting images where digitized using the NIH ImageJ software package (http://imagej.nih.gov/ij/)(see Abramoff et al., 2004).

A scale in half-millimeters divisions was included in each image. Shale preservation inevitably introduces compression-related shape variation into the analysis (see below) and, given this, we used a simple estimate of measurement error aimed at capturing the relative magnitude of measurement error compared

to within sample variance in size and shape. The raw landmark data was transformed into shape coordinates suitable for assessing differences between specimens using standard techniques (see e.g. Hunda and Hughes, 2007 for procedural details). Five specimens of different size and number of thoracic segments were chosen for evaluating the degree of measurement error (See Supp. Data 1).

The standard deviation of cranidial length estimates were less than 0.026 millimeters in all cases, and the error amounted to less than 0.6% of each linear measurement (Supp. Data 2). This is less than the 0.8% size error estimate recorded in the Fusco et al. (2004) study. Shape variance, not previously assessed for error in *A. koninckii,* was estimated by repeated digitization of fifteen cranidial landmarks for each of the five specimens, and variance values, calculated as the average Procrustes distance from the mean form, which was about 0.0005 in all cases (Supp. Data 3), using the IMP platform of David Sheets, which is a set of compiled software tools for displaying and analyzing 2-D landmark-based geometric morphometric data (http://www.canisius.edu/~sheets/morphsoft.html) (see Supp. Data 4). This is an order of magnitude lower than the variance from mean shape for members of the same meraspid segment number cohort (see analyses below), suggesting that measurement error accounts for small proportion of the observed shape variance.

Mirroring and then averaging paired landmarks across the plane of bilateral symmetry has been a widely accepted method for landmark-based analysis (Fusco et al., 2004; Zelditch et al., 2004) partly because this approach can accommodate missing landmark data on one side only. As all specimens included in this analysis preserved all landmarks the use of reflection to increase sample size was not required for this dataset. Both reflected and non-reflected landmark data were used in the analyses, and the results were compared.

The Sample

A significant disadvantage of the Na Cernidlech site is that all specimens are preserved in shale, with sclerite mineralogy recrystallized and sclerites variably fractured during compaction (Hughes, 1999; Hammer and Harper, 2006, p. 153). Such taphonomically-induced variation limits our ability to discern the fine scale patterns of biological variation evident in some trilobites preserved in silica or phosphate (c.f. Webster, 2011).

We have attempted to limit the effects of taphonomy in two ways. Firstly, following a review of *Aulacopleura*-bearing collections worldwide, we have constructed a database that is restricted to only those specimens of the highest preservational quality available. Analyses previously conducted on the original, less restrictive, dataset were repeated in order to determine whether patterns

seen in earlier work remain robustly supported. Secondly, we have considered the possible influence of taphonomy on results where appropriate.

The new dataset includes specimens selected from the holdings of National Museum of Prague (total holdings ca. 10,000 specimens), the Museum of Comparative Zoology at Harvard University (783 specimens), the Czech Geological Survey (ca. 200 specimens), the US National Museum of Natural History (55 specimens), the British Natural of Natural History (ca. 50 specimens), and the American Museum of Natural History (ca. 10 specimens). Only those specimens that were complete for all landmarks, showed no evidence of "telescoping" of the thorax or any other evident shape deformation were included, and these 352 specimens constituted approximately 4% of prone complete dorsal exoskeletons of *A. koninckii* available (Supp. Data 5). We assigned each of these specimens to one of two taphonomic grades based on their preservational quality. Taphonomic grade 1 material (N=44) included only near "perfect" specimens such as those with minor flaws unrelated to the landmarks positions, such as slight damage to the edge of the fossil, and damaged eye surface etc, which apparently had no effect on landmark position. These specimens appear to have suffered no compressional flattening. Grade 2 (N=308) material are specimens that do not have apparent shape distortion of the x,y coordinates of landmark points, have the axes of the cranidia, pygidia, and thoracic segments in precise, parallel alignment, have all pairs of landmarks

present, and possess only minor cracks, but are qualitatively slightly less well preserved than those within Grade 1, and in which we think minor flattening may have occurred.

The x-y coordinates of twenty-two landmarks were digitized for each specimen. Fifteen landmarks were assigned to the cephalic region and seven were placed on the pygidium (Fig. 1). Comparisons of variance in both size and shape between specimens assigned to Grade 1 and Grade 2 show that although Grade 1 specimens do show lower variance than Grade 2 the differences are not statistically significant for any meraspid instar (Supp. Data 6-9). Therefore we see no virtue in restricting the analysis only to Grade 1 specimens. Accordingly, all 352 specimens were subsequently treated as a single sample for statistical analysis. Although we cannot entirely exclude the influence of compression and other taphonomic process on the sample, ours does represent the highest quality of preservation of *A. koninckii* from Na Cernidlech currently available. Some of the morphological variation evident within the sample is inevitably taphonomically induced, and the extent to which this has influenced our results is discussed below.

The new dataset represent the growth history of multiple consecutive instars of *A. koninckii*, from meraspid degree 4 to later holaspid ontogenetic stages. The largest holaspid exoskeleton is 28.81 mm long and, where the meraspid growth rate to have continued throughout the holaspid phase, would represent an individual that had gone through about 32 molts since meraspid

degree 0. Out of the 352 specimens, 148 specimens (42.0%) are definitive meraspids belonging to degrees ranging between 4 to 17. From meraspid degree 9 onward the sample size is over 10 specimens per instar, so analyses of size and shape concentrated on these 9 consecutive instars. Since onset of the holaspid phase is defined by the cessation of thoracic segment addition but there are variations in number of thoracic segments in the holaspid phase for *A. koninckii* (Fusco et al. 2004), some of the smaller remaining 204 specimens (58.0%) with 18 or more thoracic segments will be late-stage meraspids. Centroid size is the square root of the sum of the squared distances of the landmarks from the centroid, is an effective measure of specimen's size that is independent of shape in landmark analyses (Bookstein, 1991). Hence below a certain size threshold (natural logarithm of cranidial centroid size of 2.2 – see Fusco et al, 2004 for the derivation of this value) we cannot be confident that all specimens with more than 18 segments are holaspides.

A comparison of the new dataset with that used in the Fusco et al. (2004) study, which is of comparable size to the new one, shows that the new dataset has significantly reduced variance in the size range of the juvenile morphs and in estimates of the shape of juvenile and mature morphs (see Supp. Data 10-11) in the new dataset. Firstly, the variance of the logarithm of the cranidial centroid size (Supp. Data 10) is notably lower. Although no significant differences between the variance estimates for each meraspid morph was detected at the 95% confidence level (two-tailed F-test for individual meraspid stage comparison:

p = 0.813 ~ 0.089), the shortest unbiased confidence intervals at 95% level and variance values are consistently lower in the new dataset. The variance in shape also displayed reduced values in the new dataset, with variance values consistently lower than the previous dataset, and the 95% confidence intervals calculated based using 1600 bootstrap resamples using DisparityBox7 were almost significantly different between the two datasets (Supp. Data 11).

These results suggest that the new dataset shows markedly less shape and size variance within individual morphs than the old one. This we interpret to be the result of the more stringent criteria applied to specimen selection and to more careful digitization. It suggests that the variation that we have now captured better approximates the original variation among the living animals.

As noted above, Hammer and Harper (2006) detected a component of variance in the positions of landmarks to indicate the action of shear stress. The third principal component (PC) of a principal component analysis (PCA) of the landmark displacement from the average shape for entire dataset revealed a pattern consistent with shear stress and accounted for 4.8% of the variation, which is comparable to but less than the 6.2% of variance value for the shear-related PC2 obtained by Hammer and Harper (2006). Both results suggest that simple shear accounts for a small proportion of total variance in the new sample, but has not been entirely excluded even in this highly selective dataset in which all specimens showing obvious shear were excluded.

Descriptive Morphology and Ontogeny of *A. koninckii*

Quantitative Description of Ontogenetic Shape Change

Ontogenetic shape changes during meraspid and holaspid growth

Ontogenetic shape variation in *A. koninckii* was achieved in several ways: shape changes within individual skeletal components, the addition of new skeletal components (e.g. trunk segments), and changes in the relative sizes of different skeletal components. This section begins with a discussion of changes in shape of cranidium throughout sampled ontogeny as this sclerite apparently maintained a stable number of segments throughout observed ontogeny. A similar condition pertains in the holaspid shape of the pygidium within any of the holaspid segment number morphs, and so this character is also explored. This is followed by a consideration of the ontogeny of overall skeletal proportions. Details of the growth patterns of individual trunk segments, and of the development of trunk articulations will be presented elsewhere.

Cranidial shape changes

Analysis of cranidial shape change was based on the landmark positions of the cranidial landmarks. These were then assessed using a thin-plate spline

analysis of the Procrustes coordinates of the landmarks of each specimen. This procedure allows shape changes to be decomposed into a series of independent movements which in combination describe the total shape variation within the sample. A PCA of the partial warp scores derived from the thin-plate spline analysis calculated about the mean shape of the whole dataset of the 15 cranidial landmarks shows that almost half of the total variance is captured by the first two principal components: Relative Warp (RW) 1 and RW2 respectively each explain 24.8% and 22.2% of the total shape variance (relative warps are the individual principal components of the total partial warp score description of shape change). Other RW's each account for less than 10% of total variance and are not considered further (See Supp. Data 12) for percentage of total variance explained). RW2 apparently suggests a pattern of very subtle elongation of the cranidium, and this might be taphonomic in origin as it mimics that known to be associated with deformation in trilobites (see Hughes and Jell, 1992; Hammer and Harper 2006). The magnitude of this effect is apparently small (Fig. 2). RW1 is a more complex pattern of shape change, and reflects expansion of the pleural regions of the cranidium relative to the glabella and palpebral lobes. Accordingly, the size of both the eye and the glabella declined relative to the overall size of the cranidium, with the intraocular free cheeks also narrowed relatively as overall relative size increased. These patterns accord with the analyses of Hammer and Harper (2006, p. 150), who reported positive allometry of the frontal area, but did not detect classic allometry in the palpebral lobe length. We concur with Hammer

and Harper (2006, p. 150) that the palpebral lobe growth relationships may be complex, but suggest that any allometry between the eye and glabellar length is quite subtle.

In order to investigate whether any of these patterns represent ontogenetic change, the partial Procrustes distance of individual specimens from the mean log cranidial centroid size (ln CCS) of the smallest three specimens in the entire dataset was calculated (Fig. 3). A significant positive relationship exists between partial Procrustes distance and ln CCS (slope 0.0365, $p < 0.0001$), and when partial warp scores from mean shape were regressed against ln CCS, 14.8% of the total shape variance was explained by the growth allometry ($p<0.000625$ for 1600 bootstraps). A deformation plot (Fig. 4) shows that the growth-related shape changes identified match those seen in Relative Warp 1 (see Fig. 2.1) and in RFTRA landmark analysis of cranidial landmarks of a different dataset (Hughes and Chapman, 1995, fig. 11). Accordingly, we consider both of these patterns to capture aspects of ontogenetic variation. Furthermore, the allometric growth vector obtained from the multivariate regression significantly differs, at the 95% confidence level, from isometry following 1600 bootstraps resamples, with the within-sample angle being 13.9° and the angle-to-isometry being 109.4°.

In order to determine if meraspid and holaspid growth phases differed in patterns of cranidial size-related shape data from 148 specimens from meraspid degrees 4 through 17 were examined (Fig. 5, Supp. Data 13). A positive

relationship between the partial Procrustes distance and ln CCS (Fig. 6) remained significant (slope 0.0314, $p<0.0001$), showing significant meraspid cranidial allometry. Multivariate regression of the partial warp scores obtained (mean shape as reference) against ln CCS is significant ($p<0.000625$ for 1600 bootstraps, Fig. 7) and explains 7.64% of total shape variance, and the vector of regression coefficient differs significantly at 95% confidence level from isometry (angle to isometry 83.0°, within sample 30.6°). The p attern of shape change identified again mimics that seen in RW1 for the total sample (Fig. 2). Likewise, as the partial Procrustes distance displays a significantly positive relationship with ln CCS only when instars separated by four or more molts are compared (Supp. Data 14), the overall amount of ontogenetically related shape change in the meraspid cranidium is quite small. Nevertheless, its close similarity to RW1 implies that the dominant pattern of shape change in the meraspid cranidium conforms to the ontogenetic trajectory. It was not possible to detect a stepped decline in the amount of shape change per meraspid instar (see Supp. Doc 14).

Similar types of shape variations seen in the meraspides are present in all holaspid morphs based on PCA of partial warp scores (Supp. Data 15-18). However, holaspides bearing 19 thoracic segments with ln CCS larger than 2.2 show no significant relationship between the partial Procrustes distance from the mean of the smallest three meraspids and ln CCS (Fig. 8). The slope of 0.0224 has a less than 95% level significant p-value of 0.0543, and an r value of 0.0488. A similar result was obtained for all the other holaspid thoracic segment number

groups (Supp. Data 19). In addition, multivariate regression of these holaspid growth data suggests that size explains only 1.50% of the total variance, which is not significant (p=0.578 for 1600 bootstraps; Fig. 9; a similar result was obtained for the other four morphs; Supp. Data 20). The lack of significant holaspid allometry makes comparison of growth trajectories between the meraspid and the holaspid phases impossible. However, for holaspids with 19 segments, when the vector of regression coefficient is compared to isometry, a significant difference at the 95% confidence level is detected (angle to isometry 101.5°, within sample 86.3°, 1600 bootstraps), and other morph s show similar results (Supp. Data 21). Accordingly, there is a suggestion of slight holaspid allometry. However, the fact that different methods of analysis of the same dataset fail to detect allometry suggest that it is, at best, subtle, as is shown by landmark deformation plot (Fig. 9). Accordingly, ontogenetically-related shape change in the holaspid phase accounts for less variation than in the meraspid phase, even though the holaspid phase likely spanned multiple instars.

Examination of the relationships between partial warp scores and ln CCS suggest that some partial warp scores have an apparently curvilinear relationship to size, but none of these relationships suggest partition of growth into distinctive phases. Accordingly, we have no indication of distinct phases of cranidial growth in any part of observed ontogeny.

Pygidial Shape Changes

For the holaspid pygidium, PCA of the partial warp scores shows that more than half of the total shape variance is explained by RW1 (54.03%) in specimens with 19 thoracic segments (with its ln CCS values higher than 2.2). The following RW2 and PW3 each explained 14.78% and 13.20% of the variance, and percentage of other relative warps fall below the 9% level (Fig. 10, Supp. Data 22). Other holaspid morphs show similar results (Supp. Data 22-23). The major component of shape variation represented by RW1 is the arching of the whole pygidium and variations in the axis-direction distance between mid-posterior end of the pygidium and anterolateral tips of the pygidium (Fig. 10, Supp. Data 23). RW2 represents variations in the relative length of the pygidium, and RW3 shows variations in the width of the pygidial axis.

There were some significant changes in the partial Procrustes distance with ln CCS for certain morphs (Fig. 11). The 19 morph and the 21 morph with its ln CCS over 2.2 each had a significant slope value of 0.0241 ($p=0.0395$, $r=0.0582$) and 0.0262 ($p=0.0044$, $r=0.2161$). Slope values of 18, 20, and 22 morphs were not significant at the 95% confidence level (Supp. Data 24). Multivariate regressions of partial warp scores against ln CCS for 19 and 21 morphs report that each growth vector explains 9.40% and 15.32% of the total variance (Fig. 12), the regressions were each significant at $p=0.001875$ (1600 bootstraps) and $p=0.003750$ (1600 bootstraps)(Supp. Data 25). In addition, the vectors of regression coefficients for the 19 morph and the 21 morph were

significantly different from isometry at the 95% confidence level (19 morph angle to isometry 90.0°, within-sample angle 46.7°; 21 morp h angle to isometry 90.0°, within-sample angle 49.6°)(Supp. Data 26).

The major shape changes with growth could not be simply linked to a single relative warp. Combined effect of relative warps could explain the arching (RW1 and RW2), shortening of axis (RW1, RW2), and narrowing of axis (RW3) seen during holaspid pygidial growth.

Exoskeletal Growth

Cephalic-trunk growth ratio

As a basis for examining how the proportions of different components of the exoskeleton varied during growth the relative lengths of the major structural components of the exoskeleton were compared (Fig. 13). Using the antilogarithm of the regression coefficient between the mean logarithm of the cranidial and exoskeletal lengths within meraspid degree 9 through 17 as the basis for estimating growth rate, the cranidial length growth rate per meraspid stage 1.083 (1.080 - 1.089) is significantly lower than the exoskeletal growth rate 1.102 (1.095 - 1.110) (see also Fusco et al., 2004). Assuming a linear relationship between these variables (see Fig. 13) the predicted cranidial-exoskeletal length ratio is 0.48 at meraspid degree 4, 0.44 at meraspid degree 9, and 0.39 at

meraspid degree 17. This is as expected because while in the cephalon growth occurred within a fixed set of segments, in the trunk growth proceeded both by increase of segment size and due to the addition of new segmental units. The pattern of decrease in the cranidial - exoskeletal length ratio slowly declines with growth from -0.008 compared to previous instar at degree 4 to -0.006 at degree 17, and this decreased rate can be expected to have declined even more in the holaspid phase due to cessation of trunk length increase through segment addition. Estimation of ratio changes in the holaspid phase (RMA regression of ln cranidial length against ln exoskeletal length for 19 morphs with ln CCS larger than 2.2) predicts values of 0.364 at exoskeletal length of 12 mm (which is about the exoskeletal length of the smallest 19 morph holaspides), and 0.358 at 20 mm (largest 19 morph holaspides).

Hence in summary, the cephalon-trunk length ratio constantly decreases with growth from the meraspid phase to the holaspid phase, and the rate of decrease for the ratio values also seems to decrease as the species grows. This might imply that the amount of shape changes per instar steadily decrease with growth instead of trilobite having two separate rates of shape changes for the meraspid phase and the holaspid phase.

Landmark-based analysis of exoskeletal shape

The complex ontogenetically dynamic nature of the trunk region complicates simple interpretation of its growth dynamics. Previous landmark-based analyses of *A. koninckii* (Hughes and Chapman, 1995, figs. 10B, 10C; Hammer and Harper, 2006, figs. 4.55, 4.57) used a scheme that combined landmarks from both the cranidium and the pygidium across different growth stages and among different holaspid segment number morphotypes to document the posterior shift and decline in relative size of the pygidium during the meraspid phase, and relative increase in size during the holaspid phase. Pygidial landmarks are apparently homologous within each holaspid segment number morphotype, but when the number of thoracic segments differed among the entities being compared, such as among the holaspid segment number morphotypes or between different meraspids degrees, the pygidium does not contain a homologous complement of segments. Accordingly, in such cases landmark-based analyses of exoskeletal growth must be understood in terms of the homology of the pygidium as an articulation-defined unit (e.g. Hughes and Chapman, 1995), not one that is homologous in terms of its constituent segments. Given these problems, and that our investigation accords with the previous analyses of overall exoskeletal growth in *A*. *koninckii*, we have not explore this issue further herein. We do, however, present an analysis of exoskeletal growth among those holaspid segment morph 19s larger than 2.2 in ln CCS value. Holaspid segment morph 19 was chosen because it is the best

represented of any of the morphs, but the patterns seen within this morph are representative of those seen in the other well-represented morphs.

In this case the most noticeable modification is the modest ontogenetic expansion of the pygidium area compared to the cranidial region, most clearly indicated by the linear outward and forward trend in the positions of landmarks that represent the anterior lateral margins of the pygidium (Fig. 14).

Characteristics of holaspid shape variation can be further analyzed by the principal component analysis (PCA) of partial warp scores calculated from the mean shape of the sample. About 67.71% of the variance is explained by the first four relative warps (RW), which account for between some 23% to 12% of overall shape variance (Supp. Data 27). Shape changes seen in RW1 closely match deformations observed with growth in *A. koninckii*. Relative warp 2 seems to represent a difference in growth rates between the cranidial and pygidial regions (Fig. 15). Relative warp 3 apparently describes minor shape variation within the cranidium and Relative warp 4 represents minor asymmetrical changes such as might result from compressional shearing. Other holaspid morphs also show similar shape variations (Supp. Data 28-31).

Shape change due to ontogeny can be evaluated by regressing partial Procrustes distances from a reference point (in this case, mean shape of three smallest specimens within the sample) against ln CS (Fig. 16). Assuming ln CS as an independent variable, the two variable shows a significant positive relationship ($r=0.4614$, $p<0.000625$). The total shape variance is 0.0848 and the

residual, non-allometric shape variance is 0.0723, hence 14.79% of the total variance is explained by the growth allometry ($p<0.000625$ from 1600 bootstraps, Fig. 17). The main allometric shape change is the expanding pygidial region compared to the cranidial area, and this trend closely follows shape changes due to Relative Warp 1 in PCA of PWS calculated from mean shape given immediately above. This, then, confirms that expansion of the relative size of the pygidium characterizes holaspid growth in this case. Other holaspid morphs display similar allometry (Supp. Data 32-33).

The significance of the allometric growth vector was tested by comparing angle to isometry with within-sample angle at 1600 bootstraps. As a result, the within-sample angle (35.2°) is significantly different at the 95% confidence level to the angle-to-isometry (76.5°). Growth vectors of other morphs also showed significant difference to isometry (Supp. Data 34).

Discussion

Our results suggest tight coordination of growth in *A*. *koninckii* and provide the oldest example of targeted growth in size and in shape yet known. They indicate that this species was able to adjust growth in its size and shape rather precisely, presumably in order to conform to an optimal condition for each particular instar. Two major questions arise from these observations. These are 1) how does this pattern of growth compare with other aspects of the

development of this animal and, 2) how does the overall pattern of growth and variation relate to the paleoenvironment in which it lived?

Curiously *Aulacopleura koninckii* is well known for its remarkable variation in the number of thoracic segments found among holaspid specimens, with variants ranging from 18 to 22 thoracic segments. No other trilobite is known to show such a wide range of variation in mature segment numbers from a single locality, even among Cambrian trilobites in which marked variation in thoracic segment numbers is well known (see Hughes et al., 1999). Previous studies of *A. koninckii* have considered the variation in mature segment number (Hughes and Chapman, 1995; Hughes et al., 1999; Fusco et al., 2004) and shown it not to be the result of lax developmental regulation, but rather that mature segment numbers were determined early in ontogeny, long before the transition to the holaspid phase. The determinant of the number in maturity may have been determined either genetically or environmentally, but it was initiated early in ontogeny. Hence it appears that development in *A. koninckii* was finely tuned for producing morphologies of the appropriate size and shape, but also allowed for some versatility in the range of form produced. At present it remains unclear whether the five mature thoracic segment morphs each represent sibling species or were rather polymorphs of a single species. The fact that the cranidial trajectory of 19 is different from that of those of 20 and 21 might provide a basis for species distinction, but as the difference is extremely subtle we do not advocate this position. More importantly, all five morphs are extremely similar in

form, differing only in the total number of a structure expressed repeatedly and iteratively in all individuals.

Accordingly, *A. koninckii* evidently employed a sophisticated regulatory network that fine-tuned development. What, then, might explain the unusual variation evident in the sample? *Aulacopleura* occurs in dense accumulations on individual bedding planes within the 1.4 meter interval of the *Aulaceopleura* shales at Na Cernedlich hill. On some bedding planes it occurs with other articulated specimens belonging to a wide variety of the Silurian shelf benthos (including echinoderms, bryozoans, brachiopods, mollusks and many other articulated trilobites), along with other material such as graptolites, chitinozoans, and pollen (see Kříž, 1992; Hughes et al., 1999). On other bedding planes *A. koninckii* is monospecific, yet occurs in great density. Bedding plane assemblages commonly differ in the mean sizes of *A. koninckii* specimens but, given the lack of physical indicators of high-energy conditions, it is unlikely that the size selectivity was the result of mechanical sorting. Accordingly, we interpret *A. koninckii* to have been an opportunistic species that flourished at the sediment-water interface at times of relatively reduced benthic oxygen conditions. Populations may have flourished relatively rapidly, but occasionally succumbed to episodes in which oxygen availability dropped below the minimum required to sustain life. The different mean sizes of *A. koninckii* specimens among the bed surfaces may reflect distinct cohorts of individuals, each of which suffered a mass kill event. Such lack of oxygen, followed by later burial, might

also explain the partially disarticulated nature of some of the individuals: the carcasses that had partially decayed before being buried.

This interpreted environment is also consistent with the morphology of *A. koninckii,* which has the olenimorphic form (Fortey and Owens, 1990) form commonly inferred to be associated with relatively reduced oxygenation (Fortey, 2000; Gaines and Droser, 2003). The olenimorphic form is rich in trunk segments with narrows axes, and this has been inferred as an adaptation to increase surface area available for respiration or for harboring chemosymbiotic microorganisms (Fortey, 2000), as such activities are considered to be associated with the exopodite branch of the appendages housed beneath each trunk segment (but also see Suzuki and Bergstrom, 2008). In this context variation in trunk segment numbers might be advantageous in conditions of relatively low oxygen availability, because more segments would also presumably imply more exopodite pairs, and thus a larger area of gaseous exchange or culturing activity. Accordingly, variation in holaspid segment numbers in *A. koninckii* could be related to variable levels of oxygen availability. If this is true we might expect to find differentiation between bedding planes in the numbers of thoracic segments, with those with higher numbers of segments presumably representing beds with less oxygen. Unfortunately, as it is not possible to collect *in situ* at the site this hypothesis remains to be tested. It is clear however, that forms with different numbers of segments do occur on the same surfaces, so any association would likely have to be detected statistically.

Conditions of reduced oxygen tension might also explain other aspects of the development of *A. koninckii.* It is likely that such conditions would present a severe metabolic challenge to all individuals and that viable morphologies would be tightly constrained to a narrow bound of variation at all stages of ontogeny. This may explain the strongly targeted pattern of development on size and shape: individuals might only be viable if they conformed to a specific shape at a specific size. Where variation was permitted, it seems, is at the later stages of development by the simple ontogenetic terminal addition or subtraction of the onset of the holaspid/epimorphic phase (Hughes et al., 2006).

Variations were evidently tolerated in the number of thoracic segments seen among mature specimens. The growth of *A*. *koninckii* thus emphasizes the point that variability is not necessarily a general characteristic of an entire animal, but can be confined to particular attributes. It suggests that variation in the number of trunk segments, which is one of the principal morphological variations seen among the clade Trilobita, may have a higher evolvability in this homonomous trilobite than other characteristics such as sclerite shape.

Conclusion

Analysis of the growth of *A*. *koninckii* with a new dataset confined to the choicest specimens available shows that the developmental of this animal in terms of the sizes and shapes of cranidium, pygidium and overall exoskeletal

proportions was both precise and tightly regulated. The animal developed gradually over a prolonged series of instars, with modest morphological changes between molts. Size growth rate per instar during the meraspid phase was constant, and variations in size and shape during the meraspid phase were also constant. Growth of cranidial size and shape was clearly targeted during the meraspid phase, and the new analysis confirms an earlier result (Fusco et al., 2004) that the number of segments in maturity was determined early in ontogeny rather than at a threshold size value when entering the mature phase. The cranidia of some of the different holaspid thoracic segment number morphs may have been slightly different in shape, suggesting that they may represent sibling species, or subtly distinct polymorphs. This pattern of growth is consistent with geological evidence suggesting that *A. kononckii* lived in an environment that experience fluctuating conditions of oxygen availability.

Systematic paleontology

Family AULACOPLEURIDAE Angelin, 1854

Genus AULACOPLEURA Hawle and Corda, 1847

AULACOPLEURA KONINCKII (Barrande, 1846)

Figures 18–21

Arethusa Koninckii BARRANDE, 1846, p. 48.

Aulacopleura (*Aulacopleura*) *koninckii koninckii* PRANTL AND PŘIBYL, 1950, p. 404–406, pl. 1, figs. 20–24, pl. 3, fig. 7 (synonymy to date); HORNÝ AND BASTL, 1970, p. 183–186.

Aulacopleura (*Aulacopleura*) *koninckii* TOMCZYKOWA, 1957, p. 132–133, pl. 3, figs. 1–2.

Otarion (*Aulacopleura*) koninckii THOMAS, 1978, p. 29, pl. 7, fig. 6; THOMAS AND OWENS, 1978, p. 68, fig. 10.

Aulacopleura koninckii ŠNAJDR, 1990, p. 22, p. 40–41, p. 176–177.

Types.—The original specimens referred to in Barrande's 1846 paper are from a locality in "Wohrada" which is the current Prague-Reporyje District of the Czech Republic. According to Horný and Bastl (1970, p. 183) this material consisted of five specimens that are stored at the National Museum of Prague. Prantl and Přibyl (1950, p.491) designated the specimen figured in the later work of Barrande (1852, pl. 18, figs. 16-17) as a lectotype without specifying a specimen number. The locality of the specimen in question is also recorded as "Wohrada" (Barrande, 1852, pl. 18 captions), but it is uncertain whether it was one of the five specimens referred to by Barrande in 1846. Currently, the specimen cannot be located from the Museum. Of the five original specimens two (L2289 and L2236) are known (Horný and Bastl, 1970, p. 183), one of which, L2236, is readily available. Consequently, the later designation of a neotype for specimen L2022 (IT 278) by Horný and Bastl (1970, p. 185) is erroneous. In

addition, specimen L2022 (IT278) is from a different locality, that of Lodenice, Beroun District (Horný and Bastl, 1970, p. 185). Therefore, specimen L2236 is proposed to be designated as the lectotype.

Locality.—Na Cernidlech hill, Lodenice, Beroun District, Czech Republic. "*Aulacopleura* shales", upper 1.4 meter interval of the Motol Formation, *Testograptus testis* zone, Homerian, Wenlock, Silurian.

Diagnosis.—*Aulacopleura* with 18 to 22 thoracic segments in the holaspid phase; narrow subrectangular glabella that weakly tapers anteriorly; hypostome with constriction at the anterior portion of the middle body; small eyes with sagittal length shorter than half of glabellar length throughout ontogeny, anterior point of eye reaching height of preglabellar furrow.

Description.—Exoskeleton ovate in outline; sagittal length about 65% of cranidial width across posterior border.

Cephalon semicircular in outline; sagittal length about 55% of cranidal width across posterior border; sagittal length about 35% of exoskeletal sagittal length. Cephalon highly convex; dorsal surface convexity of glabella and LO follow curvature of genal field. Anterior genal field gently sloping ventrally compared to more steeply sloping lateral genal field. Posterior genal field sloping steeper adaxially. Caecal pits spaced evenly throughout on genal field, roughly equal number of pits throughout growth; pits apparently slightly smaller on posterior fixigenae, about 40 pits per 1 mm^2 in specimen with cranidial length 5.6 mm. Anterior and lateral cephalic border narrow, tubular. Anterior cephalic border

arched dorsally in anterior view. Posterior cephalic border shortens (exsag.) adaxially. Anterior and lateral cephalic border furrows very short (sag.), moderately to weekly narrow (tr.), incised. Posterior cephalic border furrow lengthens (exsag.) abaxially. Genal spine directed posteriorly, about two times the width (tr.) of lateral cephalic border at base, tapered evenly, continuing curvature of cephalic outline. Anterior branches of facial suture diverge at 20º to axis anteriorly, rapidly converge at 90º to axial line slightly before reaching border furrows. Posterior branches of facial suture diverge at 60º to axis posteriorly; terminate at genal angle. Frontal area length about 45% of cranidial length.

Holochroal eyes small, kidney-shaped; length about 15% of cranidial length. Anterior end of eye located at about 85% of glabellar length. Posterior end of eye located at about 50% of glabellar length. Distance of eye to axis about 40% of cranidial width across posterior border. Eye surface and palpebral lobe hemispherical, upstanding. Base of hemisphere elevated vertically above genal field about half the height of hemisphere. Eye socle and eye socle furrow continuous in curvature; slopes conically near genal field at about 60º to plane of genal field, weakly expanding abaxially just below eye surface. Visual field spans slightly below horizontal plane to 90º above. Overlap of visual fields from paired eyes about 35º front and back. Hexagonal close packing of lenses with at least 20 lenses at basal horizontal row and at least 20 horizontal rows of lenses. Eye ridge perpendicular to sagittal axis; intersects anterior portion of eye. Lateral axial

furrows narrow (tr.), very deeply incised, gently bowed out around L1; preglabellar furrow gently arching anteriorly.

LO sagittal anterior arched forward. LO length shortens (exsag.) abaxially. Maximum LO length about 10% of cranidial length. Cephalic median organ quincuncial; occurs as four small outer tubercles and a larger central one on flat surface, located slightly anterior to sagittal mid-point of LO. SO deepest near axial furrow; shallowing sagittally. Glabella trapezoidal in outline. Sagittal anterior arch of glabella continuous with that of preglabellar field and of LO. Glabella widest at posterior of L1. Glabellar length and width about 45% and 25% of cranidial length and width, respectively. Width of anterior glabella across eye ridges about 75% of maximum glabellar width. Glabella tapering anteriorly at about 5º to sagittal axis. L1 teardrop shaped, slightly protruding laterally in glabellar outline. S1 deep near lateral axial furrow, shallowing adaxially, fully isolating L1, in contact with medial SO. L2 very weakly represented by small notch opposite middle (exsag.) of eye.

Hypostome subrectangular. Maximum width near posterolateral margin at about 65% of sagittal length. Anterior margin gently arching anteriorly in the middle, extended into long (sag.) anterior wings laterally. Lateral margin parallel to sagittal axis behind about anterior 35% of sagittal length, slightly divergent posteriorly at about anterior 60% of sagittal length. Posterior margin semicircular to trapezoidal. Posterolateral spines absent. Anterior border as long as posterior border at long sagittal axis; abruptly lengthens abaxially near anterior wing,

continuous with anterior lobe and anterior wing. Lateral border slopes steeply into lateral border furrow, slightly narrower than posterior border is long. Posterior border uniform in length, flange-like. Border furrow at anterolateral corners converge anteriorly at about 30º to sagittal axis behind anterior wing, deep, trough-like, uniformly wide; defines bottleneck shaped anterior lobe. Lateral border furrow deeply incised, narrow opposite anterior lobe, as wide as posterior border furrow at posterolateral region. Posterior border furrow deep, uniformly long. Middle body constricted at about anterior 20% of sagittal length to minimum width of about 65% of maximum middle body width, slightly inflated transversely anterior to narrowest position. Middle body length about 90% of hypostomal sagittal length. Middle body width about 70% of hypostomal maximum width near posterolateral margin. Surface sculpture weakly defined fingerprint-like pattern. Middle furrow slit-like on internal mold, converging posteriorly at about 45º to sagittal axis opposite inflection point of lateral border, isolated from sagittal axis.

Trunk with homonomous segments. Number of thoracic segments in epimorphic forms ranges from 18 through 22. Thoracic length about 55 to 60% of exoskeletal length with segment-poor specimens closer to about 55% and with segment-rich ones closer to about 60%. Maximum length and width of trunk at seventh from anterior segment. Ratio of axial to pleural width about 25% near middle. Outer portion of pleura beyond fulcrum about 40% of pleural width. Pleural furrow long (exsag.) and parallel to segment margin in inner portion, shortening (exsag.) abaxially in outer portion. Length of posterior band increasing

abaxially in outer portion of pleura. Pleural extremity of anterior segment developed into pointed tip. Pleural margin of posterior segments rounded. Axis tapering posteriorly, occupying about 25% of segment width on seventh segment from anterior. Axial ring flexed posteriorly at abaxial margin then curving anteriorly near axis to form weak W shape in dorsal view. Weak median tubercle visible in some segments. Articulating furrow short (sag. and exsag.).

Pygidium semielliptical in outline with sagittal length about 25% of maximum pygidial width. Pygidial border narrow, of uniform thickness. Pygidial border furrow very shallow and narrow. Inner portion of pleural field horizontal width between fulcra at thorax-pygidium boundary about 65% of maximum pygidial width. Pleural furrow up to four pairs, more prominent anteriorly, deep, wide. Anterior band length about 50% of posterior band at inner portion of pleural field, about the same length at outer portion of pleural field. Interpleural furrow up to four pairs, deep, narrow at inner portion of pleural field; starts to widen abaxially at inner-outer boundary of pleural field. Subtriangular depression at pygidial border furrow. Moderately clear relation between axial and pleural segments. Pygidial axis conical in outline, gently converges posteriorly. Posterior portion broadly rounded. Length of pygidial axis about 80% of pygidial length. Width of pygidial axis about 20% of maximum pygidial width. Axis composed of four or up to six axial rings and a terminal axial piece. Inter-ring furrow short (sag. and exsag.), incised, slightly bulging anteriorly.

Ontogeny.—Other than the addition of trunk segments in the meraspid phase, and the complementary release of anterior pygidial segments into the thorax, no other ontogenetic changes in nominal or ordinal characters could be detected from meraspid degree 4 to the largest holaspid. Such changes that do occur are related to the overall sizes of individual sclerites, the numbers trunk segments, and to their allocation to the pygidium or thorax.

As described above, during the meraspid phase the relative length of the cranidial frontal area expands, the front of the glabellar becomes less rounded, and the posterior broader widens and moves slightly anteriorly. Thus in larger forms the glabella and eyes are relatively smaller than those in earlier meraspides.

With regard to the overall shape of the exoskeleton, the major ontogenetic change is the expansion of the area occupied by the thorax during meraspid ontogeny, and the relative decline in the size of the pygidium during this phase. This decline is related to the fact that although the pygidium did increase in size during the meraspid phase, such increase was mitigated by loss of the anteriormost pygidial segment into the thorax at each meraspid molt. Thus, as a proportion of the total exoskeleton, the pygidium became both narrower and shorter during later meraspid growth. This growth relationship changed during the holaspid phase, because the pygidium was no longer releasing or adding segments, and its constituent segments thus increased in size. The details of individual trunk segment growth rates will be discussed in a separate publication.

Details of the average length and width values for various stages are described below based on are the antilogarithm of average logarithm values for each meraspid stage. Values inside the parentheses are lower and upper limits at 95 percent confidence level.

The sagittal length of the exoskeleton ranges from 1.72 mm to 28.81 mm for the specimens that represent meraspid degree 4 through 17, and holaspides with 18, 19, 20, 21, or 22 thoracic segments. The average sagittal length of the exoskeleton is 3.22 mm (3.04 - 3.41 mm) at meraspid degree 9 and 7.10 mm (6.85 - 7.35 mm) at degree 17. The exoskeletal width-length ratio decreases with growth from 0.72 (0.67 - 0.78) at meraspid degree 9 to 0.68 (0.66 - 0.71) at degree 17, and the ratio is around 0.63 to 0.66 in the holaspid phase. The sagittal cranidial length ranges from 0.93 mm to 9.61 mm, with the average value of 1.42 mm (1.34 - 1.50 mm) at meraspid degree 9 and 2.76 mm (2.65 - 2.87 mm) at degree 17. The proportion of cephalic length to the exoskeletal length decreases with growth from 0.44 (0.43 - 0.45) at meraspid degree 9 to 0.39 (0.38 - 0.40) at degree 17, and the proportion decreases with growth from about 0.36 to 0.34 in the holaspid phase.

The sagittal pygidial length ranges from 0.36 mm to 2.72 mm, with the average value of 0.56 mm (0.50 - 0.62 mm) at meraspid degree 9 and 0.61 mm (0.57 - 0.65 mm) at degree 17. As noted above the pygidial length in the meraspid phase is the net effect of anteriormost pygidial segment loss and gain of a new pygidial segment near the posterior between instars. The general trend

in the ratio of pygidial length to the exoskeletal length is a decrease in the meraspid phase and an increase in the holaspid phase. It decreases from 0.17 (0.16 - 0.18) at meraspid degree 9 to 0.09 (0.08 - 0.09) at degree 17, then increases in the holaspid phase from about 0.08 to 0.11. Although with large overlaps in values, the proportional length of pygidium compared to exoskeletal length in the segment-rich holaspides tends to be smaller than the ratio from the segment-poor ones. Holaspides with 19 thoracic segments have the pygidial-exoskeletal length ratio of about 0.08 to 0.12, 20 and 21 morphs have 0.07 to 0.11, and 22 morphs have values of 0.06 to 0.10. This is because at any given holaspid size the pygidia of the segment poor forms have been longer in the holaspid growth mode.

The length-width ratio of the cranidium decreases with growth from 0.61 (0.57 - 0.65) at meraspid degree 9 to 0.57 (0.55 -0.59) at degree 17, and becomes around 0.54 to 0.55 in the holaspid phase. Length of the glabella including the occipital ring ranges from 0.58 mm to 5.22 mm, and the average value is 0.86 mm (0.81 - 0.91 mm) at meraspid degree 9 and 1.56 mm (1.51 - 1.62 mm) at degree 17. The proportion of glabellar length to the cranidial length decreases with growth in the meraspid phase from 0.60 (0.58 - 0.63) at meraspid degree 9, 0.57 (0.55 - 0.59) at degree 17, and becomes around 0.53 to 0.54 in the holaspid phase. The proportion of the glabellar width (at the base of the occipital ring) to the cranidial width remains relatively constant during growth with observed values of 0.26 (0.24 - 0.26) at meraspid degree 9, 0.25 (0.24 - 0.25) at

meraspid degree 17, and around 0.23 in the holaspid phase. The glabellar width-length ratio increases from 0.70 (0.63 - 0.77) at meraspid degree 9 to 0.76 (0.72 - 0.81) at degree 17, and becomes around 0.79 to 0.81 in the holaspid phase. The sagittal occipital ring length ranges from 0.10 mm to 1.10 mm, with the average value of 0.14 mm (0.12 - 0.15 mm) at meraspid degree 9 and 0.23 mm (0.21 - 0.27 mm) at degree 17. The ratio of occipital ring length to the glabellar length remains relatively constant during growth with observed values of 0.16 (0.15-0.17) at meraspid degree 9, 0.15 (0.13 - 0.17) at degree 17, and around 0.15 in the holaspid phase.

The length-width ratio of the pygidium generally decreases in the meraspid phase from about 0.32 at meraspid degree 9, to about 0.27 at meraspid degree 17, and becomes around 0.25 to 0.26 in the holaspid phase. The proportion of pygidial axis length to the pygidial length remains relatively constant during growth with observed values of 0.80 (0.77 - 0.83) at meraspid degree 9, 0.80 (0.76 - 0.83) at meraspid degree 17, and around 0.80 to 0.82 in the holaspid phase. The general trend in the ratio of pygidial axis width to the pygidial width in the meraspid phase is an increase from 0.20 (0.18 - 0.21) at meraspid degree 9 to 0.22 (0.22 - 0.23) at meraspid degree 17. In the holaspid phase, the ratio decreases from around 0.23 to 0.20 for the 19-thoracic segment specimens, 0.24 to 0.20 for the 20 morphs, and 0.24 to 0.21 for 21 and 22 morphs.

The sagittal length of the eye ranges from 0.15 mm to 1.56 mm, with the average sagittal length of the eye being 0.28 mm (0.24 - 0.32 mm) at meraspid degree 9 and 0.51 mm (0.47 - 0.55 mm) at degree 17. The proportional length of the eye compared to glabellar length remains relatively constant during the meraspid phase with observed values of 0.33 (0.30 - 0.36) at meraspid degrees 9 and 17. In the holaspid phase, the ratio decreases with growth from about 0.30 to 0.25. The ratio of eye's distance to the axial furrow and the cranidial width decreases with growth in the meraspid phase from 0.13 (0.11 - 0.15) at meraspid degree 9 to 0.12 (0.10 - 0.13) at meraspid degree 17. The ratio remains constant, at about 0.11, during the holaspid phase. The ratio of the glabellar width at the eye ridges and the glabellar width at the base of the occipital ring remains constant during growth with observed values of 0.77 (0.73 - 0.83) at meraspid degree 9, 0.79 (0.77 - 0.81) at meraspid degree 17, and around 0.81 to 0.82 in the holaspid phase.

The ratio of the distance between anteriormost points of facial sutures and the cranidial width remains constant during growth with observed values of 0.39 (0.39 - 0.44) at meraspid degree 9, 0.40 (0.39 - 0.42) at meraspid degree 17, and about 0.40 in the holaspid phase.

Discussion.—*Aulacopleura* species are known quite widely around the word and from Llandovery to Upper Devonian in age (see Adrain and Chatterton, 1995): the upper Llandovery (Šnajdr, 1975), Wenlock (Barrande, 1846; Přibyl et al., 1985), Lochkovian (Barrande, 1872), and Pragian (Přibyl, 1947) of the Czech

Republic; the Upper Silurian (Kegel, 1927), Eifelian (Roemer, 1850), the Upper Devonian (Barrande, 1868) of Germany; Wenlock of France (Chaubet, 1937); Caradoc of Scotland (Přibyl, 1947); Eifelian of Morocco (Alberti, 1969); Tremadoc (?) of China (Lu, 1975); Llandovery of northwestern Canada (Adrain and Chatterton, 1995).

Prantl and Přibyl (1950) classified a subspecies *Aulacopleura* (*Aulacopleura*) *koninckі haueri* (Frech, 1887) based on a specimen from the Carnic Alps of Australia and Italy and a Silurian Czech specimen of *Arethusina Koninckі* var. *peralta* Katzer, 1895. According to Prantl and Přibyl (1950), the subspecies is different from *A*. *koninckii* based on having a more convex cephalon, a prominent process at the mid-anterior border of the cephalon, a shorter librigenal spine, and extra pair of glabellar furrows.

Based on specimens from the Na Cernidlech hill, *A*. *koninckii* is different from all other *Aulacopleura* species by having 18 through 22 thoracic segments in the holaspid phase, a narrow subrectangular glabella that weakly tapers anteriorly, a hypostome with middle body that is pinched at the anterior portion, and anteriorly positioned eyes that are less than half the length of the glabella.

References

ABRAMOFF, M. D., P. J. MAGALHAES, AND S. J. RAM. 2004. Image Processing with ImageJ. Biophotonics International, 11:36–42.

ADRAIN, J. M., AND B. D. E. CHATTERTON. 1995. Aulacopleurine trilobites from the Llandovery of northwestern Canada. Journal of Paleontology, 69:326–340.

ALBERTI, G. K. B. 1969. Trilobiten des jüngeren Siluriums sowie des Unter- und Mitteldevons. I. Abhandlungen der Senckenbergischen Naturforschenden Gesellschaft, 520:1–692.

ANGELIN, N. P. 1851–1878. Palaeontologia Scandinavica. Pars 1. Crustacea Formations Transitionis [fasc. 1 (1851): Palaeontologia Suecica, p. 1–24, pls 1–24; fasc. 2 (1854): Palaeontologia Scandinavica p. i–ix, 21–92, pls. 25–41 (Academiae Regiae Scientarum Suecanae: Holmiae); republished in combined and revised form (1878): G. Lindström, ed., x+96p, 41pls]. Norstedt and Söner, Stockholm.

BARRANDE, J. 1846. Notice Préliminaire sur le Système Silurien et les Trilobites de Bohême. Hirschfield, Leipzig, 96 p.

BARRANDE, J. 1852. Système Silurien du Centre de la Bohême. I. Recherches Paléontologiques, vol. 1 (Crustacés: Trilobites). Prague and Paris, 935 p.

BARRANDE, J. 1868. Silurische Fauna aus der Umgebung von Hof in Bayern. Neues Jahrbuch für Mineralogie, Geologie und Paläontologie, 1868: 641–696.

BARRANDE, J. 1872. Système Silurien du Centre de la Bohême. I. Recherches Paléontologiques, supplement au vol. 1 (Trilobites, Crustacés divers et Poissons). Prague and Paris, 647 p.

BOOKSTEIN, F. L. 1991. Morphometric Tools for Landmark Data. Cambridge University Press, New York, 435 p.

CHAUBET, M. C. 1937. Contribution á l'étude géologique du Gothlandien du versant méridional de la Montagne Noire. Travaux du Laboratoire de Géologie de la Faculté des Sciences de Montpellier, Mémoire, 1:1–224.

FATKA, O., AND M. MERGL. 2009. The "microcontinent" Perunica; status and story 15 years after conception, p. 65–101. *In* M. G. Bassett (ed.), Early Palaeozoic Peri-Gondwana Terranes: New Insights from Tectonics and Biogeography. Geological Society, London, Special Publications, 325.

FORTEY, R. 2000. Olenid trilobites: The oldest known chemoautotrophic symbionts? Proceedings of the National Academy of Sciences of the United States of America, 97:6574–6578.

FORTEY, R. A., AND R. M. OWENS. 1990. Trilobites, p. 121–142. *In* K. J. McNamara (ed.), Evolutionary Trends. Belhaven Press, London.

FRECH, G. 1887. Über das Devon der Ostalpen nebst Bemerkungen über das Silur und einem paläontologischen Anhang. Zeitschrift der Deutschen Geologischen Gesellschaft, 39:659–738.

FUSCO, G., N. C. HUGHES, M. WEBSTER, AND A. MINELLI. 2004. Exploring developmental modes in a fossil arthropod: Growth and trunk segmentation of the trilobite *Aulacopleura konincki*. American Naturalist, 163:167–183.

GAINES, R. R., AND M. L. DROSER. 2003. Paleoecology of the familiar trilobite *Elrathia kingii*: an early exaerobic inhabitant. Geology, 31:941–944.

HAMMER, Ø., AND D. A. T. HARPER. 2006. Paleontological Data Analysis. Blackwell Publishing, Malden, MA, 351 p.

HAWLE, I., AND A. J. C. CORDA. 1847. Prodrom einer Monographie der böhmischen Trilobiten. Abhandlugen Koeniglichen Boehmischen Gesellschaft der Wissenschaften. J.G. Calve, Prague, 176 p.

HORNÝ, R., AND F. BASTL. 1970. Type specimens of fossils in the National Museum, Prague. Volume 1, Trilobita. Museum of Natural History, Prague, 354 p.

HUGHES, N. C. 1999. Statistical and imaging methods applied to deformed fossils, p. 127–155. *In* D. A. T. Harper (ed.), Numerical Palaeobiology. John Wiley, London.

HUGHES, N. C., AND R. E. CHAPMAN. 1995. Growth and variation in the Silurian proetide trilobite *Aulacopleura konincki* and its implications for trilobite palaeobiology. Lethaia, 28:333–353.

HUGHES, N. C., AND R. E. CHAPMAN. 2001. Morphometry and phylogeny in the resolution of paleobiological problems; unlocking the evolutionary

significance of an assemblage of Silurian trilobites. Topics in Geobiology, 19:29–54.

HUGHES, N. C., R. E. CHAPMAN, AND J. M. ADRAIN. 1999. The stability of thoracic segmentation in trilobites: a case study in developmental and ecological constraints. Evolution and Development, 1:24–35.

HUGHES, N. C., AND P. A. JELL. 1992. A statistical/computer-graphic technique for assessing variation in tectonically deformed fossils and its application to Cambrian trilobites from Kashmir. Lethaia, 25:317–330.

HUGHES, N. C., A. MINELLI, AND G. FUSCO. 2006. The ontogeny of trilobite segmentation: a comparative approach. Paleobiology, 32:602–627.

HUNDA, B. R., AND N. C. HUGHES. 2007. Evaluating paedomorphic heterochrony in trilobites: the case of the diminutive trilobite *Flexicalymene retrorsa minuens* from the Cincinnatian Series (Upper Ordovician), Cincinnati region. Evolution and Development, 9:483–498.

KATZER, F. 1895. Beiträge zur Palaeontologie des älteren Palaeozoicums in Mittelböhmen. Verlag der könig. Böhmischen Gessellschaft der Wissenschaften, 14:1–17.

KEGEL, W. 1927. Über obersilurische Trilobiten aus dem Harz und dem Rheinischen Schiefergebirge. Jahrbuch der Preußischen Geologischen Landesanstalt zu Berlin, 48:616–647.

KŘÍŽ, J. 1992. Silurian Field Excursions: Prague Basin (Barrandian), Bohemia. National Museum of Wales, Geological Series, 13, 111 p.

LU, Y. 1975. Ordovician trilobite faunas of central and southwestern China. Palaeontologia Sinica, New Series B, 11:1–463.

PRANTL, F., AND A. PŘIBYL. 1950. Revise čeledi Otarionidae R. a E. Richter z českého siluru a devonu (Trilobitae). Sborníku Státního Geologického, Ústavu Československé Republiky, oddíl paleontologický, 17:353–512.

PŘIBYL, A. 1947. *Aulacopleura* and the Otarionidae. Journal of Paleontology, 21:537–545.

PŘIBYL, A., J. VANĚK, AND F. HORBINGER. 1985. New taxa of Proetacea (Trilobita) from the Silurian and Devonian of Bohemia. Časopis pro Mineralogii a Geologii, 30:237–251.

ROEMER, F. A. 1850. Beiträge zur geologischen Kenntnis des nord-westlichen Harzgebirges. Palaeontographica, 3:1–67.

ŠNAJDR, M. 1975. New Trilobita from the Llandovery at Hyskov in the Beroun Area Central Bohemia Czechoslovakia. Věstník Ústředního ústavu geologického, 50:311–316.

ŠNAJDR, M. 1990. Bohemian Trilobites. Geological Survey, Prague, 265 p.

SOKAL, R. R., AND F. J. ROHLF. 1981. Biometry the Principles and Practice of Statistics in Biological Research (second edition). W. H. Freeman and Company, San Francisco, 859 p.

STORCH, P. 2006. Facies development, depositional settings and sequence stratigraphy across the Ordovician-Silurian boundary; a new perspective from the Barrandian area of the Czech Republic. Geological Journal, 41:163–192.

SUZUKI, Y., AND J. BERGSTROM. 2008. Respiration in trilobites: a reevaluation. GFF, 130:211–229.

THOMAS, A. T. 1978. British Wenlock Trilobites Part 1. Palaeontographical Society Monographs, 132: 56 p.

THOMAS, A. T., AND R. M. OWENS. 1978. A review of the trilobite family Aulacopleuridae. Palaeontology, 21:65-82.

TOMCZYKOWA, E. 1957. Trilobites from the Wenlock and lower Ludlow graptolitic shale of the Święty Krzyż Mountains. Instytut Geologiczny Biuletyn, 122:83–143.

WEBSTER, M. 2011. The structure of cranidial shape variation in three early ptychoparioid trilobite species from the Dyeran-Delamaran (traditional "Lower-Middle" Cambrian) boundary interval of Nevada, U.S.A. Journal of Paleontology, 85:179–225.

ZELDITCH, M., D. SWIDERSKI, D. H. SHEETS, AND W. FINK. 2004. Geometric Morphometrics for Biologists. Academic Press, San Diego, 416 p.

Figures

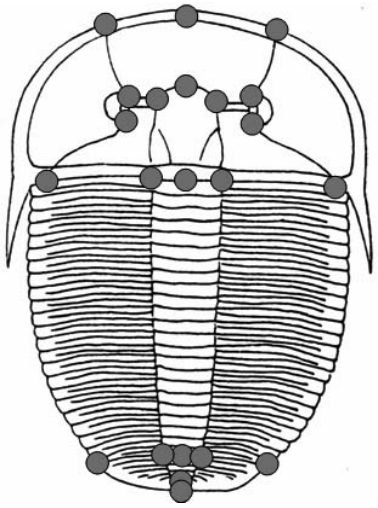

FIGURE 1—Grey dots show position of fifteen cranidial landmarks and seven pygidial landmarks on the dorsal exoskeleton of *Aulacopleura koninckii* (modified from Hughes and Chapman, 1995, fig. 3).

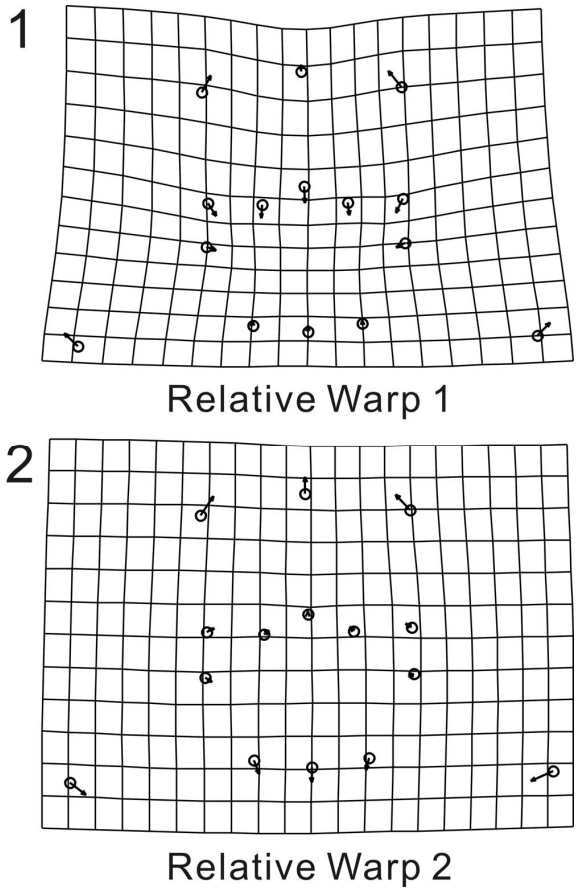

FIGURE 2—Thin-plate spline deformation grid of relative warps for the 15 cranidial landmarks of all specimens of holaspides and meraspides (N=352): *1*, Shape variation related to relative warp 1 (24.80% of total variance explained, depicting size of the pleural region relative to the glabella and the palpebral lobes); *2*, Shape variation related to relative warp 2 (22.23% of total variance explained, depicting very subtle elongation of the cranidium).

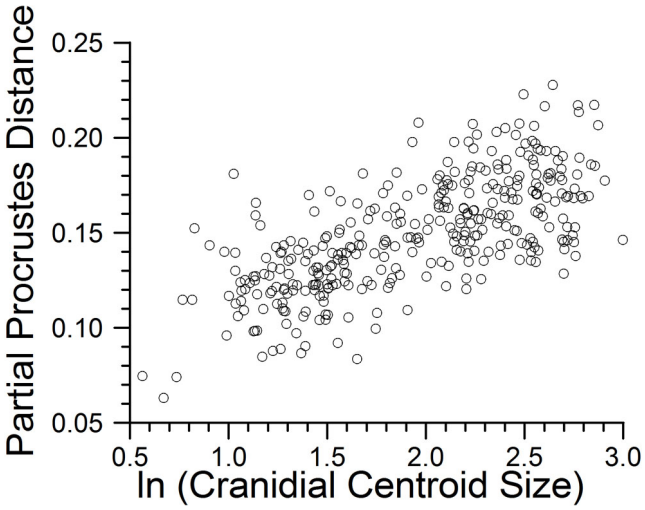

FIGURE 3—Partial Procrustes distance from the reference (mean shape of the smallest three specimens) of 15 cranidial landmarks for all specimens of holaspides and meraspides (N=352). Regression of partial Procrustes distance against logarithm of cranidial centroid size is significant (slope=0.0365, $P<0.0001$, $r=0.4808$).

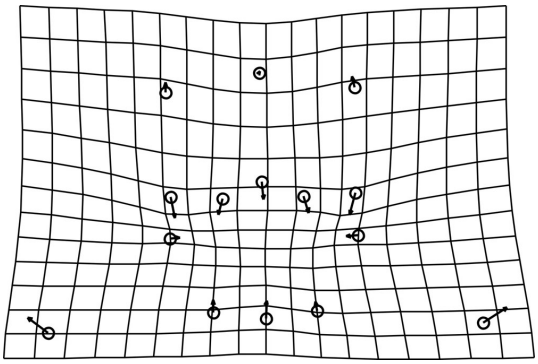

FIGURE 4—Thin-plate spline deformation grid of shape changes with growth for the 15 cranidial landmarks of all specimens of holaspides and meraspides (N=352). Partial warp scores are regressed in a multivariate regression against ln centroid size, and 14.7687% of total shape variance (based on summed squared residuals expressed in Procrustes units) is explained by the allometry ($p<0.000625$ from 1600 bootstraps).

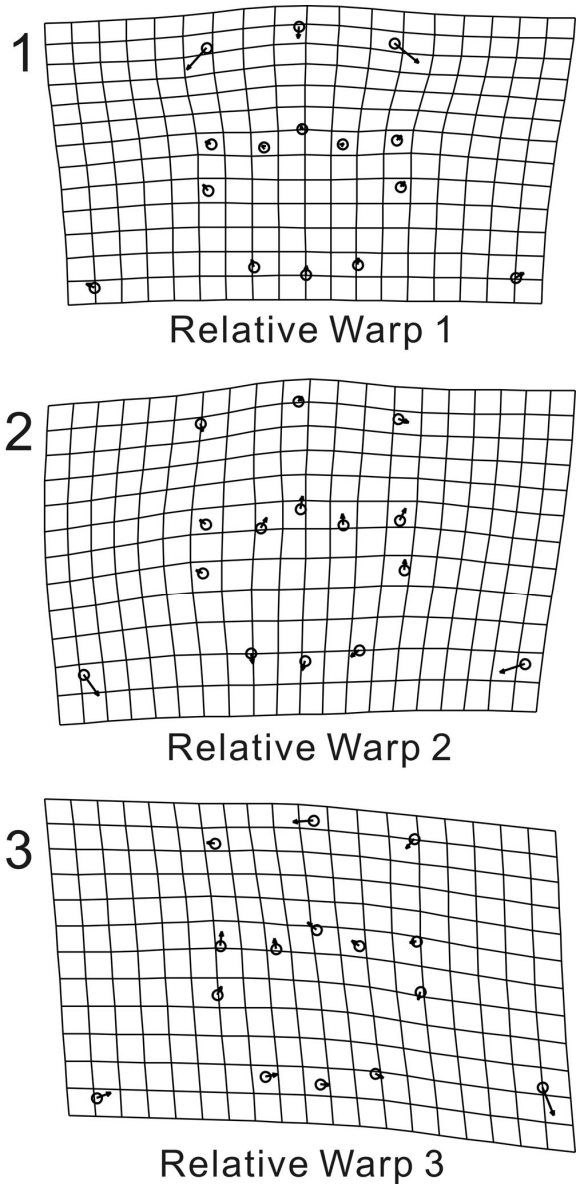

FIGURE 5—Thin-plate spline deformation grid of relative warps for the 15 cranidial landmarks of meraspides from meraspid degree 4 through 17 (N=148): *1*, Shape variation related to relative warp 1 (26.35% of total variance explained, depicting variations in the anterior width between the facial sutures); *2*, Shape

variation related to relative warp 2 (16.58% of total variance explained, depicting size of the pleural region relative to the glabella and the palpebral lobes); *3*, Shape variation related to relative warp 3 (10.31% of total variance explained, depicting effects of shearing).

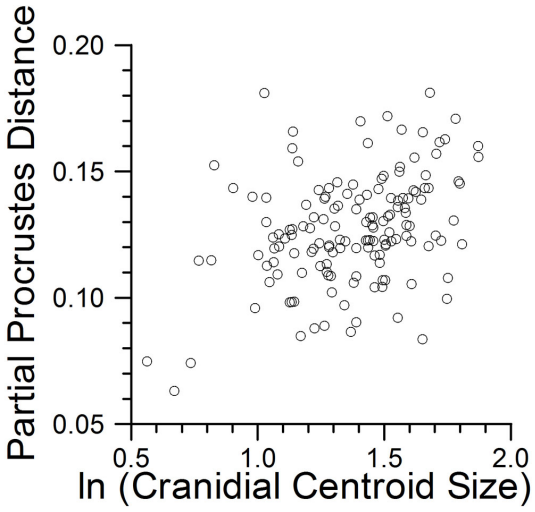

FIGURE 6—Partial Procrustes distance from the reference (mean shape of the smallest three specimens) of 15 cranidial landmarks for specimens of meraspides from meraspid degree 4 through 17 (N=148). Regression of partial Procrustes distance against logarithm of cranidial centroid size is significant (slope=0.0314, P<0.0001, r=0.1377).

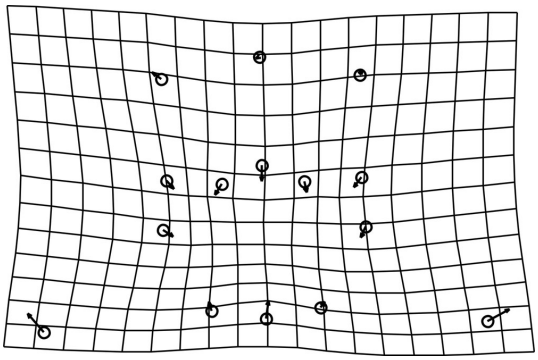

FIGURE 7—Thin-plate spline deformation grid of shape changes with growth for the 15 cranidial landmarks for specimens of meraspides from meraspid degree 4 through 17 (N=148). Partial warp scores are regressed in a multivariate regression against ln centroid size, and 7.6358% of total shape variance (based on summed squared residuals expressed in Procrustes units) is explained by the allometry ($p<0.000625$ from 1600 bootstraps).

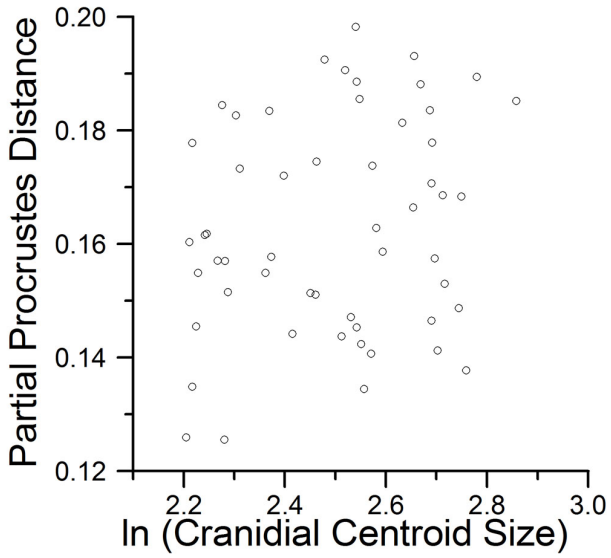

FIGURE 8—Partial Procrustes distance from the reference (mean shape of the smallest three specimens) of 15 cranidial landmarks for holaspid specimens of 19 morphs with its ln CCS value more than 2.2 (N=54). Regression of partial Procrustes distance against logarithm of cranidial centroid size is not significant at the 95% confidence level (slope=0.0224, P=0.0543, r=0.0488)

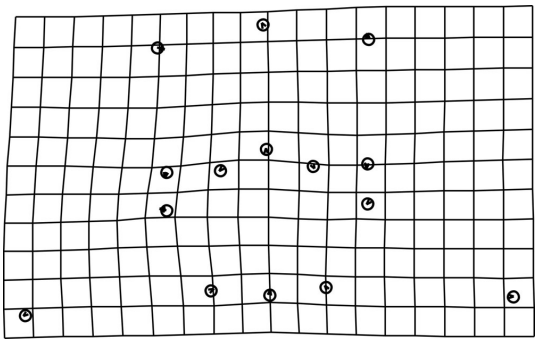

FIGURE 9—Thin-plate spline deformation grid of shape changes with growth of 15 cranidial landmarks for holaspid specimens of 19 morphs with its ln CCS value more than 2.2 (N=54). Partial warp scores are regressed in a multivariate regression against ln centroid size, and total shape variance (based on summed squared residuals expressed in Procrustes units) explained by the allometry is not significant at the 95% confidence level (1.5045% of total variance explained, p=0. 578125 from 1600 bootstraps).

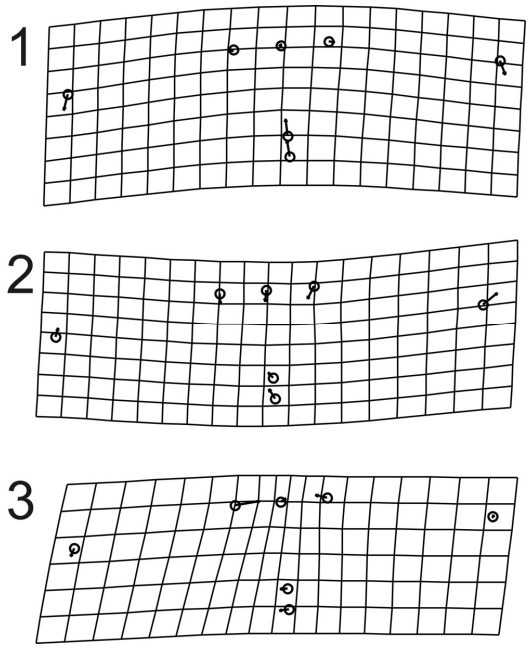

FIGURE 10—Thin-plate spline deformation grid of relative warps for the 7 pygidial landmarks for holaspid specimens of 19 morphs with its ln CCS value more than 2.2 (N=54): *1*, Shape variation related to relative warp 1 (54.03% of total variance explained); *2*, Shape variation related to relative warp 2 (14.78% of total variance explained); 3, Shape variation related to relative warp 3 (13.19% of total variance explained).

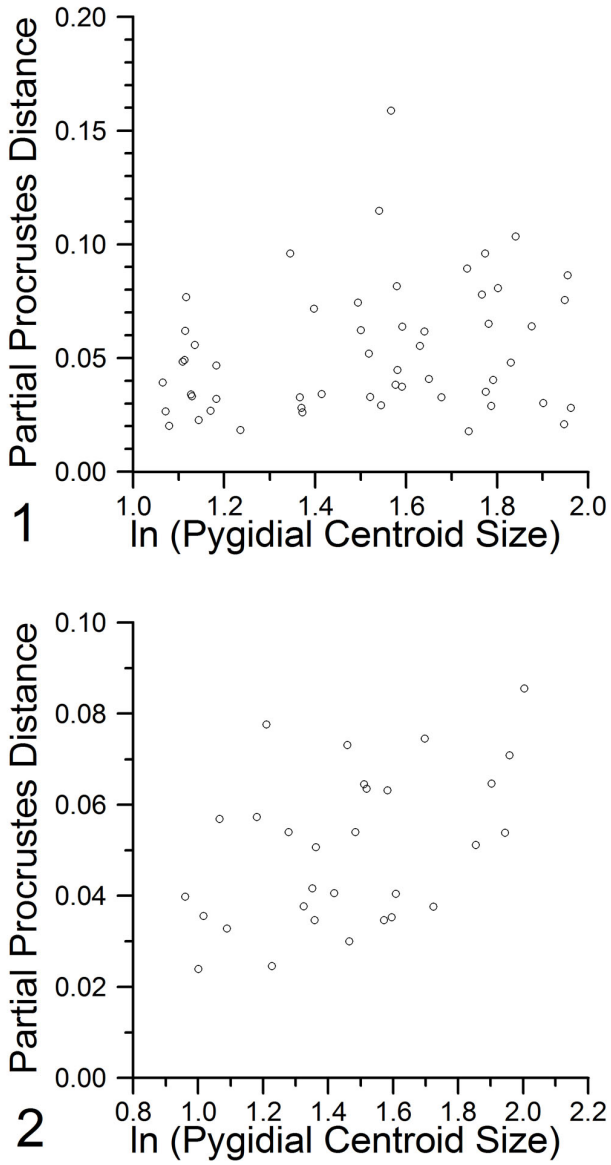

FIGURE 11—Partial Procrustes distance from the reference (mean shape of the smallest three specimens) of 7 pygidial landmarks for holaspid specimens of 19 morphs (N=54) and 21 morphs (N=30) with its ln CCS value more than 2.2. Regression of partial Procrustes distance against logarithm of pygidial centroid

size is significant. *1*, 19 morphs (slope=0.0241, P=0.0395, r=0.2412); *2*, 21 morphs (slope=0.0262, P=0.0044, r=0.4649)

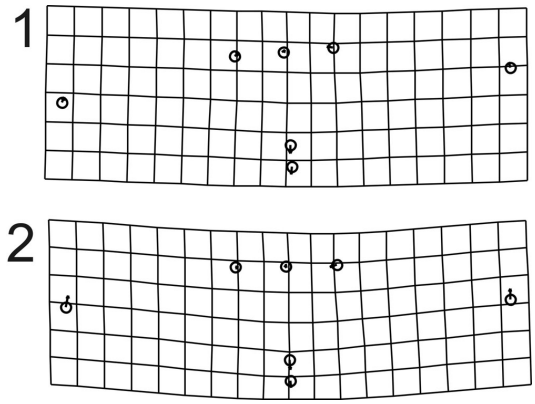

FIGURE 12—Thin-plate spline deformation grid of shape changes with growth of 7 pygidial landmarks for holaspid specimens of 19 morphs (N=54) and 21 morphs (N=30) with its ln CCS value more than 2.2. Partial warp scores are regressed in a multivariate regression against ln pygidial centroid size. *1*, 19 morph, 9.40% of total shape variance (based on summed squared residuals expressed in Procrustes units) is explained by the allometry (P=0.001875 from 1600 bootstraps); *2*, 21 morph, 15.32% of total shape variance is explained by the allometry (P=0.003750 from 1600 bootstraps).

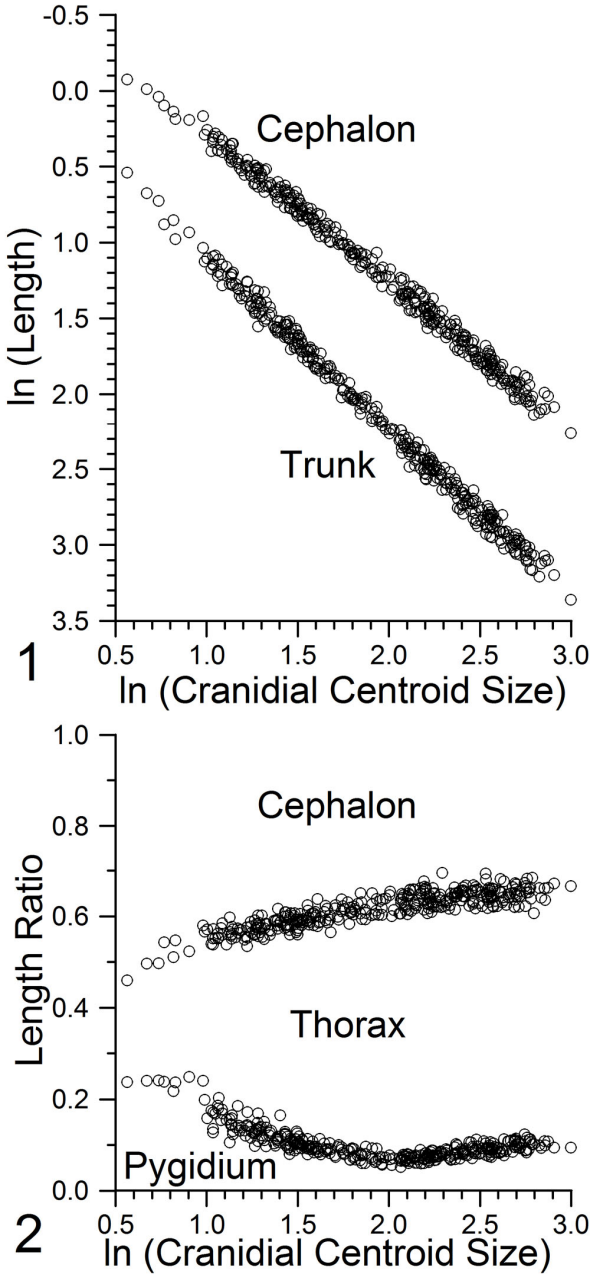

FIGURE 13—Changes in length ratios of cephalon, thorax, and pygidium with growth for all meraspid and holaspid specimens (N=352): *1*, Bivariate plot of ln

cephalic length and ln trunk length against ln cranidial centroid size; *2*, Changes in ratio of cephalic-thoracic-pygidial length with growth.

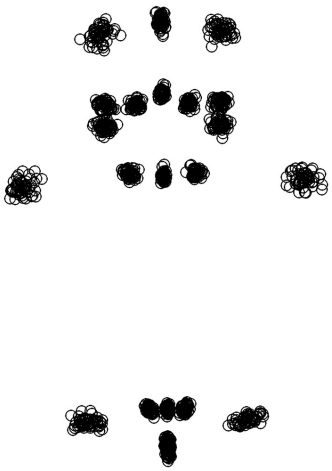

FIGURE 14—Procrustes superimposition of 22 exoskeletal landmarks for holaspid specimens of 19 morphs with its ln CCS value more than 2.2 (N=54).

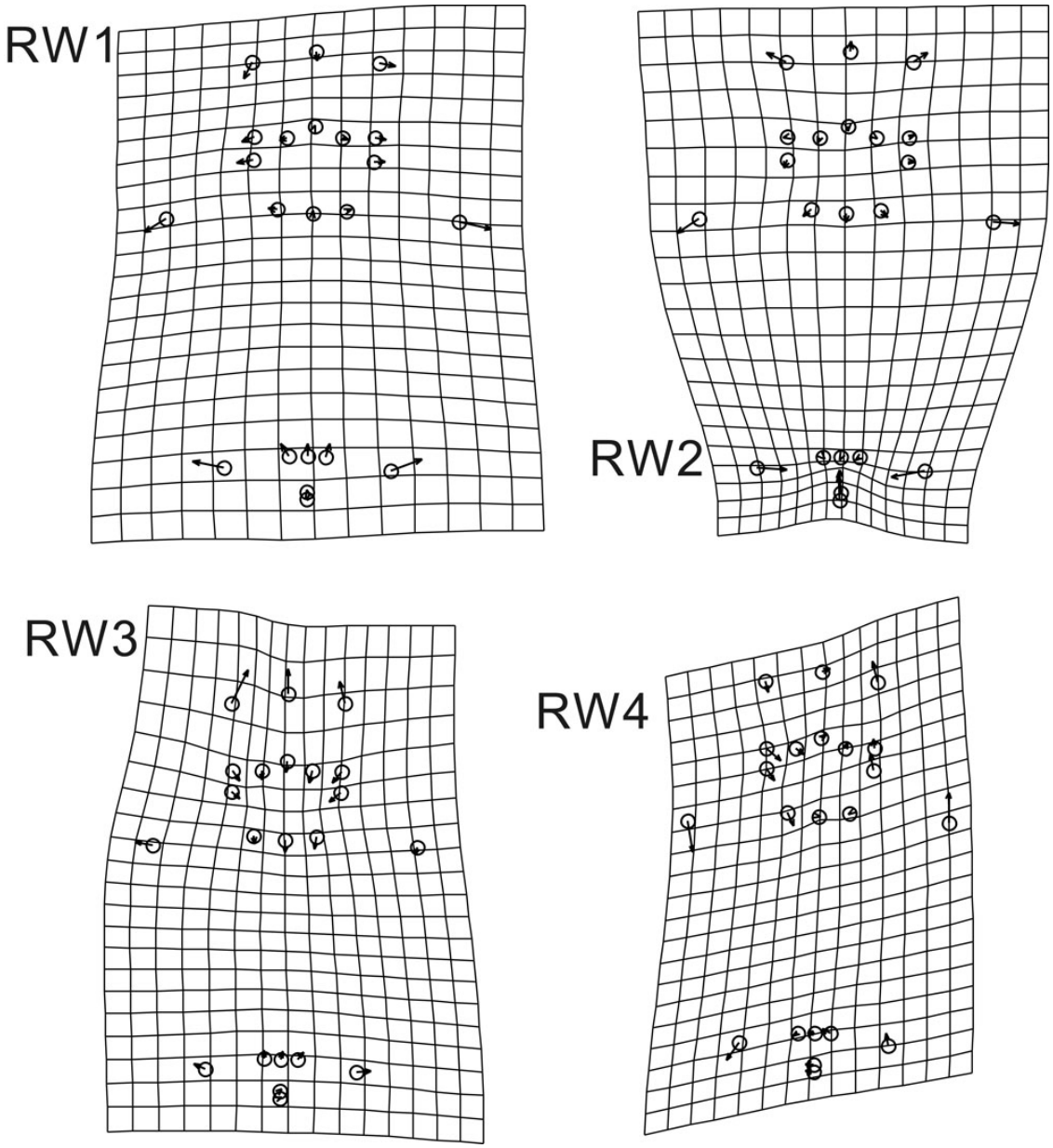

FIGURE 15—Thin-plate spline deformation grid of relative warps of 22 exoskeletal landmarks for holaspid specimens of 19 morphs with its ln CCS value more than 2.2 (N=54): *1*, Shape variation related to relative warp 1 (22.94% of

total variance explained); *2*, Shape variation related to relative warp 2 (16.71% of total variance explained)); *3*, Shape variation related to relative warp 3 (15.90% of total variance explained); *4*, Shape variation related to relative warp 4 (12.16% of total variance explained).

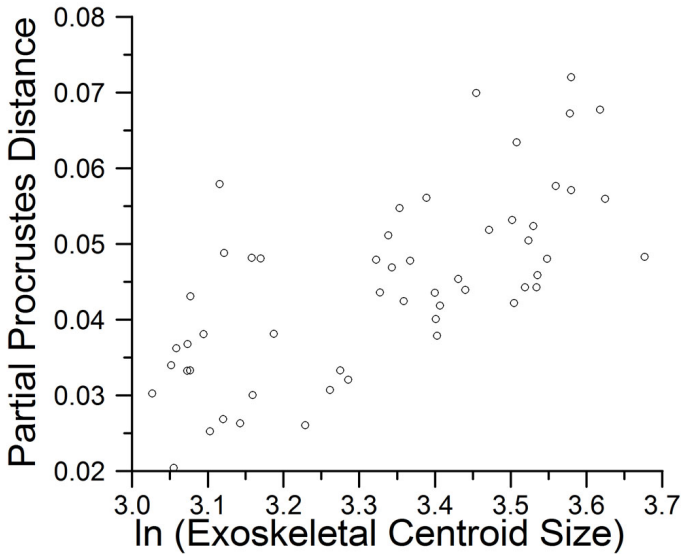

FIGURE 16—Partial Procrustes distance from the reference (mean shape of the smallest three specimens) of 22 exoskeletal landmarks for holaspid specimens of 19 morphs with its ln CCS value more than 2.2 (N=54). Regression of partial Procrustes distance against logarithm of cranidial centroid size is significant (slope=0.0425, P<0.0001, r=0.6792).

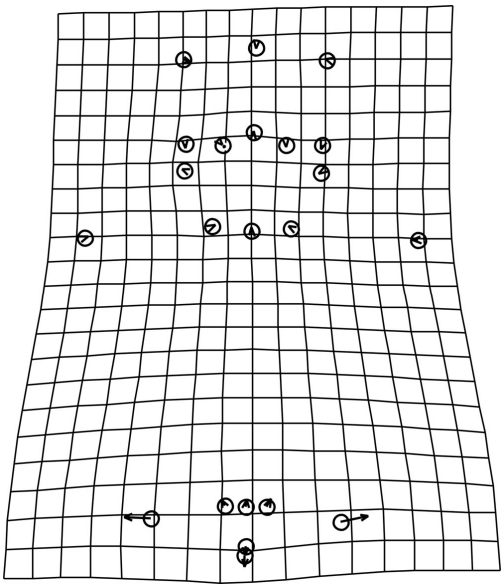

FIGURE 17—Thin-plate spline deformation grid of shape changes with growth of 22 exoskeletal landmarks for holaspid specimens of 19 morphs with its ln CCS value more than 2.2 (N=54). Partial warp scores are regressed in a multivariate regression against ln centroid size, and 14.7893% of total shape variance (based on summed squared residuals expressed in Procrustes units) is explained by the allometry ($p<0.000625$ from 1600 bootstraps).

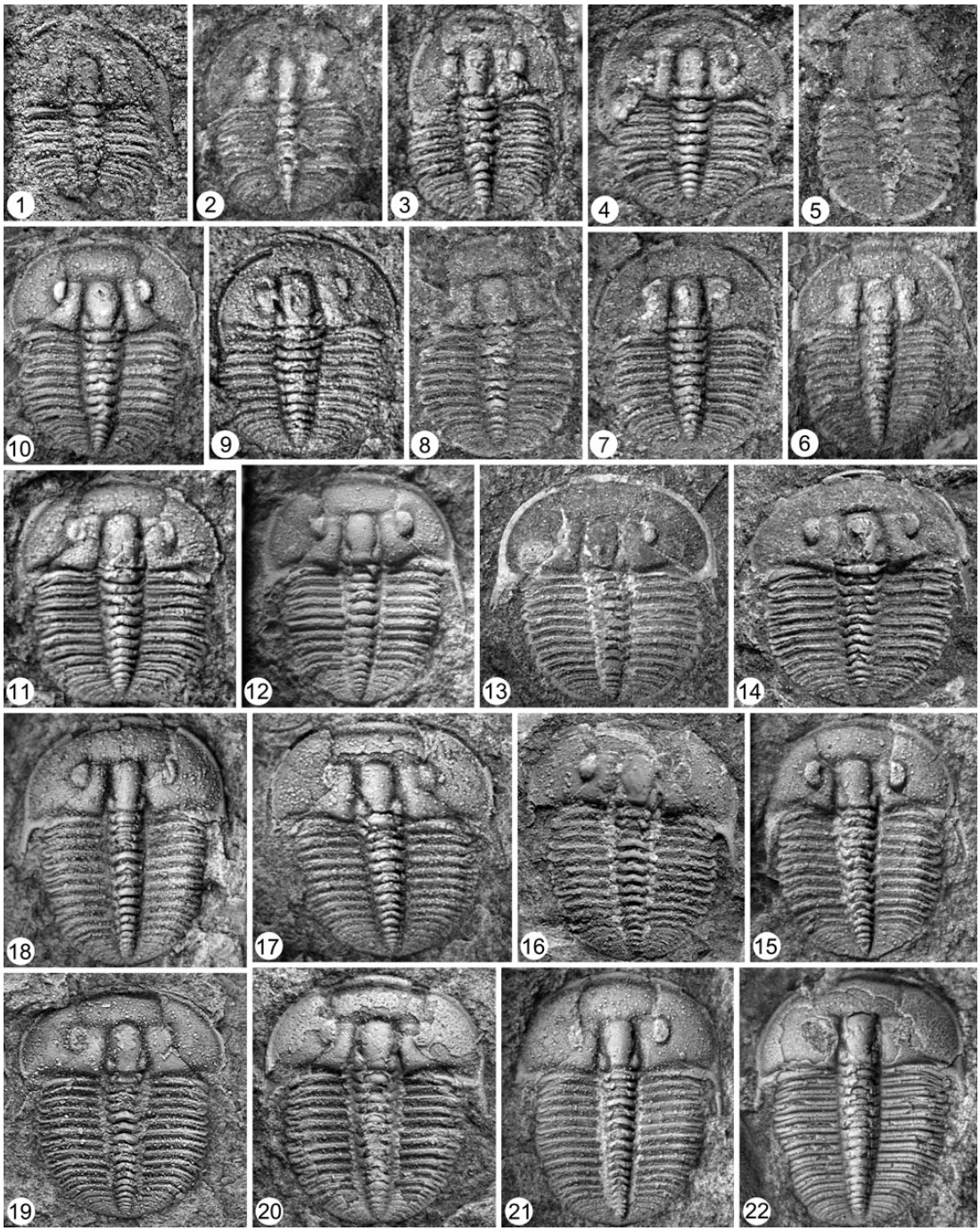
1
2
3
4
5
10
9
8
7
6
11
12
13
14
18
17
16
15
19
20
21
22

FIGURE 18—*Aulacopleura koninckii* (Barrande, 1846) from Na Cernidlech hill, Czech Republic; specimens coated with magnesium oxide prior to photography: *1*, meraspid degree 4, MCZ177964 ×16.4; *2*, meraspid degree 4, NMPL39407 ×15.2; *3*, meraspid degree 5, NMPL40040A ×15.6; *4*, meraspid degree 5, NMPL39950 ×15.2; *5*, meraspid degree 6, NHM 42364.3 ×13.6; *6*, meraspid degree 6, NMPL39916 ×12.0; *7*, meraspid degree 6, NMPL2234(L12783) ×14.0; *8*, meraspid degree 7, NHM42364.1 ×12.0; *9*, meraspid degree 7, NMPL2243 ×15.6; *10*, meraspid degree 8, NMPL39957 ×12.0; *11*, meraspid degree 8, NMPL40082 ×14.4; *12*, meraspid degree 9, NMPL40035 ×11.2; *13*, meraspid degree 9, NMPL39924 ×10.8; *14*, meraspid degree 9, MCZ116103 ×11.2; *15*, meraspid degree 10, NMPL40028 ×10.0; *16*, meraspid degree 10, NHM42365.5 ×10.4; *17*, meraspid degree 10, NMPL39949 ×10.0; *18*, meraspid degree 11, NMPL40079 ×9.6; *19*, meraspid degree 11, NMNH475176 ×8.8; *20*, meraspid degree 11, MCZ116205 ×9.2; *21*, meraspid degree 12, NMPL39961 ×8.8; *22*, meraspid degree 12, NMPL40023 ×8.8.

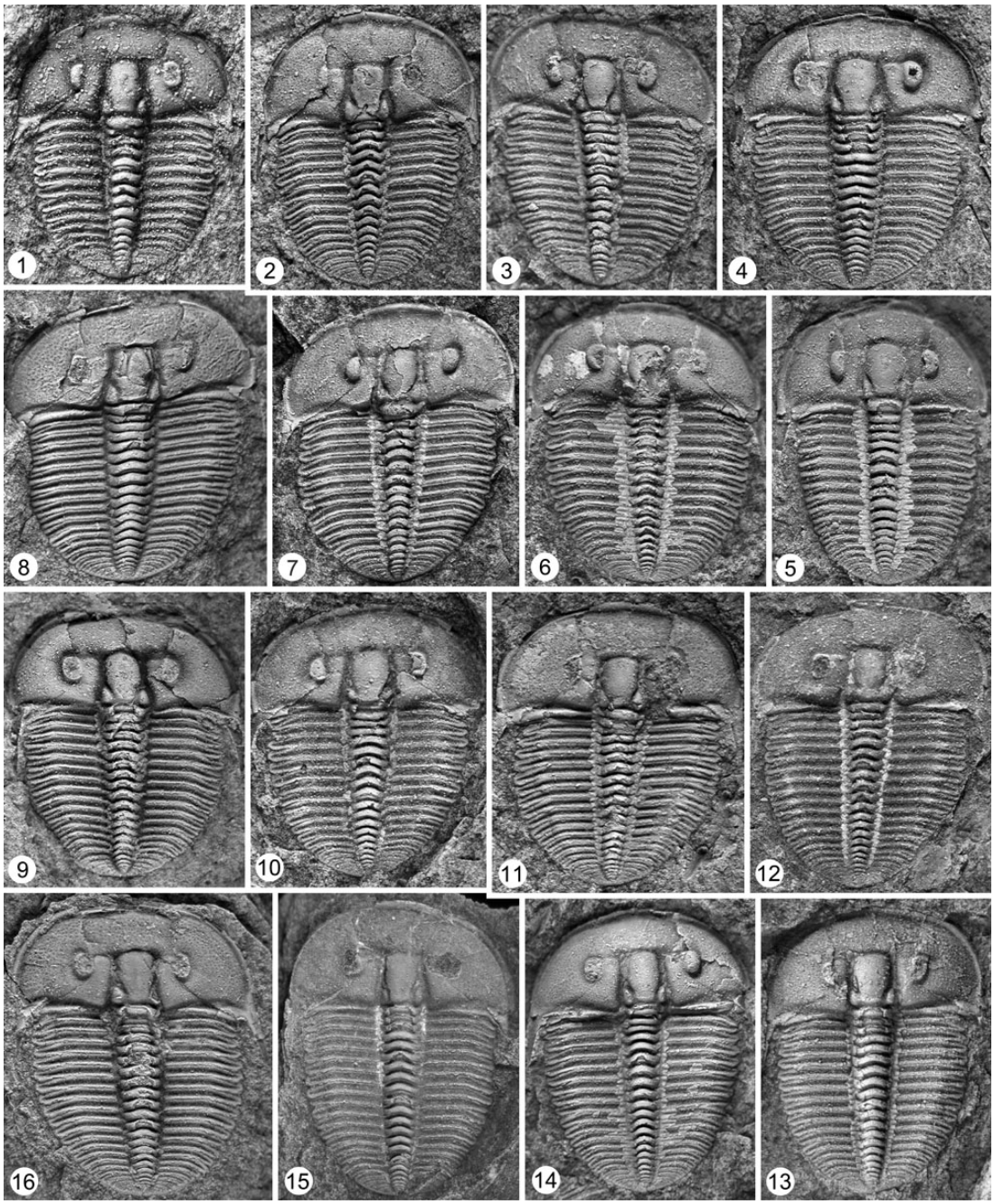

FIGURE 19—*Aulacopleura koninckii* (Barrande, 1846) from Na Cernidlech hill, Czech Republic; specimens coated with magnesium oxide prior to photography:

1, meraspid degree 12, NHM42365 ×10.8; *2*, meraspid degree 13, MCZ177963 ×7.6; *3*, meraspid degree 13, MCZ115992 ×8.4; *4*, meraspid degree 13, MCZ116201 ×8.8; *5*, meraspid degree 14, MCZ115990 ×7.6; *6*, meraspid degree 14, MCZ115987 ×7.2; *7*, meraspid degree 14, MCZ177744 ×8.0; *8*, meraspid degree 15, MCZ114948 ×7.6; *9*, meraspid degree 15, NMNH475182(475181) ×6.4; *10*, meraspid degree 15, MCZ116186 ×8.0; *11*, meraspid degree 16, MCZ114936 ×6.8; *12*, meraspid degree 16, MCZ116055 ×6.8; *13*, meraspid degree 16, NMPL40073 ×6.8; *14*, meraspid degree 17, MCZ115406 ×6.0; *15*, meraspid degree 17, MCZ116087 ×6.0; *16*, meraspid degree 17, MCZ177982 ×6.4.

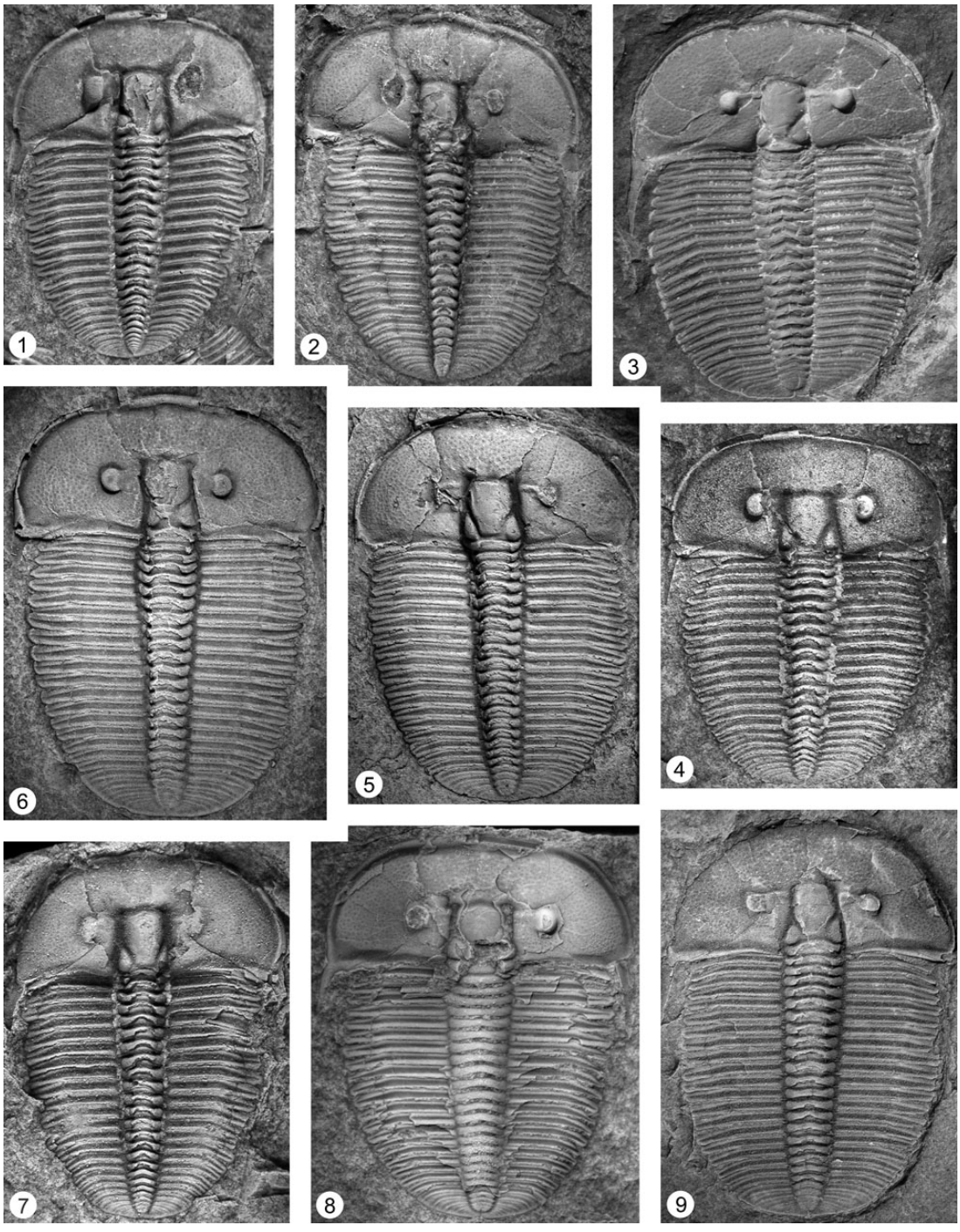
1
2
3
6
5
4
7
8
9

FIGURE 20—*Aulacopleura koninckii* (Barrande, 1846) from Na Cernidlech hill, Czech Republic; specimens coated with magnesium oxide prior to photography: *1*, 18 thoracic segments, MCZ116174 ×6.5; *2*, 18 thoracic segments, NHM59826.6 ×3.7; *3*, 18 thoracic segments, NMPL2229 3.×2.7; *4*, 19 thoracic segments, MCZ103490 ×4.6; *5*, 19 thoracic segments, MCZ114934 ×3.4; *6*, 19 thoracic segments, MCZ116074 ×3.1; *7*, 20 thoracic segments, NMNH475499 ×5.0; *8*, 20 thoracic segments, NMPL39840 ×3.4; *9*, 20 thoracic segments, NHM59836(59826Q) ×3.2.

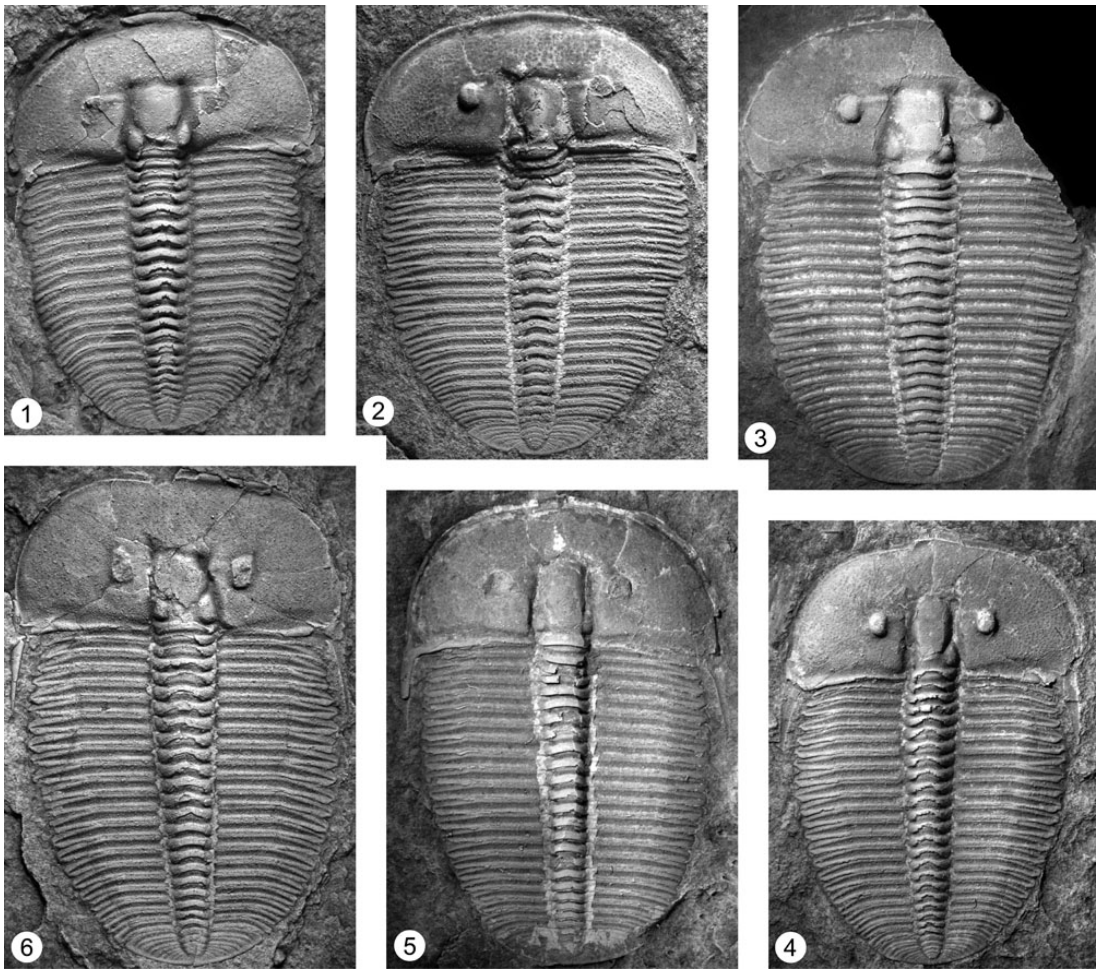

FIGURE 21—*Aulacopleura koninckii* (Barrande, 1846) from Na Cernidlech hill, Czech Republic; specimens coated with magnesium oxide prior to photography: 1, 21 thoracic segments, MCZ114950 ×5.1; 2, 21 thoracic segments, MCZ176470 ×3.8; 3, 21 thoracic segments, NMPL39848 ×3.2; 4, 22 thoracic segments, NMPL39850 ×3.6; 5, 22 thoracic segments, NMPL39851 ×3.3; 6, 22

Supplementary Data

Supplementary data 1.

The following specimens were used for analysis of measurement error: MCZ 114934-19-5-G3, MCZ 114935-21-5-G3, MCZ 114944-22-5-G3, MCZ 115987-14-7-G3, and NHM 475176-11-7-G3. All were taphonomic grade 2. Each of these five specimens was coated, mounted, photographed, and digitized, and this process was repeated ten times per specimen over the course of several days.

Supplementary data 2.

Specimen ID	morph	mean cranidial length [mm]	standard deviation	coefficient of variation
NHM 475176	11	1.606419	0.013396	0.833878 %
MCZ 115987	14	2.108004	0.022652	1.074578 %
MCZ 114934	19	5.773783	0.017109	0.296314 %
MCZ 114935	21	4.138166	0.015362	0.371233 %
MCZ 114944	22	5.114652	0.025710	0.502675 %

Size measurement error estimation from mounting, photographing, and digitizing ten times each of five specimens selected.

Supplementary data 3.

Specimen ID	morph	distance-based (Foote) disparity	95% confidence (lower)	95% confidence (upper)
NHM 475176	11	0.000672	0.000410	0.000774
MCZ 115987	14	0.000471	0.000276	0.000548
MCZ 114934	19	0.000344	0.000838	0.001668
MCZ 114935	21	0.001471	0.000124	0.000356
MCZ 114944	22	0.000270	0.000149	0.000424

Shape variance as represented by partial Procrustes distances from the mean form of five specimens selected for analysis of measurement error. Each of the five specimens was digitized ten times. Non-reflected 15 landmarks on the cephalon were used in the analysis. Confidence values calculated based on 900 bootstrap resamples using DisparityBox6i.

Supplementary data 4.

IMP series programs used in the study.

1. Program CoordGen7 changes raw mm-scale x and y coordinates of specimens into coordinates of generalized least square Procrustes superimposition. Each specimen's coordinates are first translated to have its centroid at origin, then coordinates are scaled to unit centroid size, and specimens are rotated to minimize the summed squared distances between homologous landmarks (partial Procrustes distances).

2. Program DisparityBox7 measures morphological diversity of a group based on landmark data. In this study, each specimen's partial Procrustes distance from the mean shape is used as a unit of shape variance within an instar. The "bootstrap within-group disparity" option is used to calculate the variance and the 95% confidence interval.

3. Program PCAGen7 first translates the shape differences between individual specimen and the mean shape in a Procrustes superimposition into mathematically independent style of deformation (called the partial warp scores) that also sets the correct number of degree of freedom for statistical tests, and then runs principal component analysis on the partial warp scores. Each principal component is called a relative warp, and PCAGen7 measures which relative warp explains what percentage of the total shape variance.

4. In program Regress7, partial warp scores are regressed in a multivariate regression against ln centroid size to produce a vector of regression coefficients. Proportion of total shape variance explained by this allometry is then calculated, and significance of the multivariate regression is determined by bootstrapping method. Partial Procrustes distance can also be calculated through the program.

5. Program TwoGroup7 measures partial Procrustes distances between group mean shapes, and compares significance of within-group and between-group variances through bootstrapping method.

6. Program VecCompare7 tests significance of the difference between two vectors of regression coefficients by comparing the angle between the two groups and within-group angles through bootstrapping method. It could also calculate whether the growth vector is significantly different from isometry.

7. Program BigFix6 reflects paired homologous landmarks across an axial midline and calculate the average position for each paired landmarks.

Supplementary data 5.

Details on the specimen number, collector, and locality information (N=352).

1. National Museum of Prague (N=166)

   Lxxxxx - Lodenice-Cernidla (N=166)

2. Museum of Comparative Zoology at Harvard University (N=142)

   MCZ1xxxxx - Lodenice, Schary collection (N=142)

3. Czech Geological Survey (N=21)

   OTxxxx - Lodenice-Cernidla, Vanek collection (N=4)

   Pxxxx - Lodenice-Cernidla, Horný collection, 1976 (N=17)

4. US National Museum of Natural History (N=12)

   xxxxxx - Lodenitz (N=12)

5. British Natural of Natural History (N=11)

   xxxxx.x - Lodenitz (N=11)

Supplementary data 6.

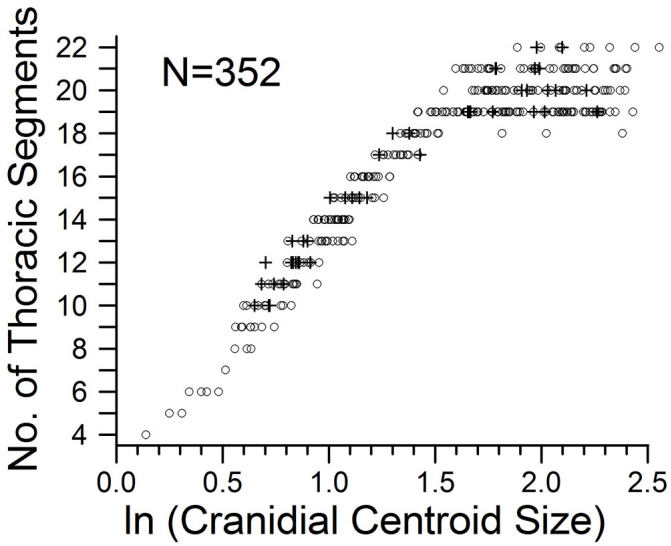

Logarithm of cranidial centroid size for the two preservational grades of the new dataset showing that the two grades do not differ markedly invariance. Among the 15 landmarks of the cranidium, 6 paired homologous landmarks were reflected across an axial midline for the analysis and averaged. Cross marks are grade 1 materials, and circles indicate grade 2 specimens.

Supplementary data 7.

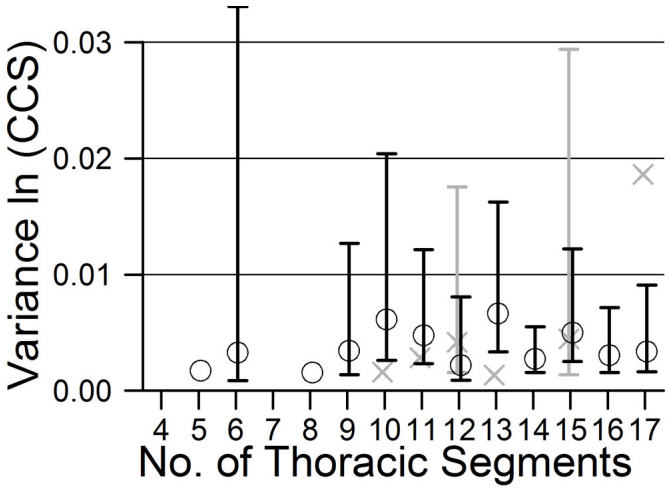

Variance of logarithm of cranidial centroid size for the two preservational grades of the new dataset suggesting that both grades show similar variance. Among the 15 landmarks of the cranidium, 6 paired homologous landmarks were reflected across an axial midline for the analysis and averaged, using the program BigFix6 in the morphometrics series IMP. Gray x marks are grade 1 materials, and black circles indicate grade 2 specimens. Bars are 95% confidence intervals by the method of shortest unbiased confidence intervals (Sokal and Rohlf, 1981).

Supplementary data 8.

morph	Grade 1 Variance	Grade 1 n	Grade 2 Variance	Grade 2 n	F	P
10	0.001594	3	0.006161	9	3.864070	0.443592
11	0.002837	3	0.004755	13	1.676275	0.867515
12	0.004167	7	0.002203	8	1.891765	0.423577
13	0.001338	3	0.006648	14	4.966794	**0.049956**
15	0.004463	5	0.004993	14	1.118769	1.000000
17	0.018650	2	0.003393	12	5.496959	0.077717

Two-tailed F-test at 95% confidence level of differences in size variance between grade 1 and 2 for those morphs with sufficient sample size in both grades from the new dataset. Among the 15 landmarks in the cephalon, 6 paired homologous landmarks were reflected across an axial midline for the analysis. “Morph” refers to the number of thoracic segments, n to the number of individuals. No significant difference in variance is detected between the grade 1 and 2 materials except for the 13 thoracic segment number morph.

Supplementary data 9.

Comparison of the instar variance in the cranidial shape of specimens belonging to grades 1 and 2, computed via the partial Procrustes distance of individual specimen to the consensus of all specimens in Procrustes superimposition for each instar (Zelditch et al., 2004, p. 297–302), revealed that there was no significant difference. When the size variance of ln CCS (mirrored) value for each meraspid stage (10, 11, 12, 15, 17) is compared for G1 and G2, there was no significant difference (Supp. Data 6-8).

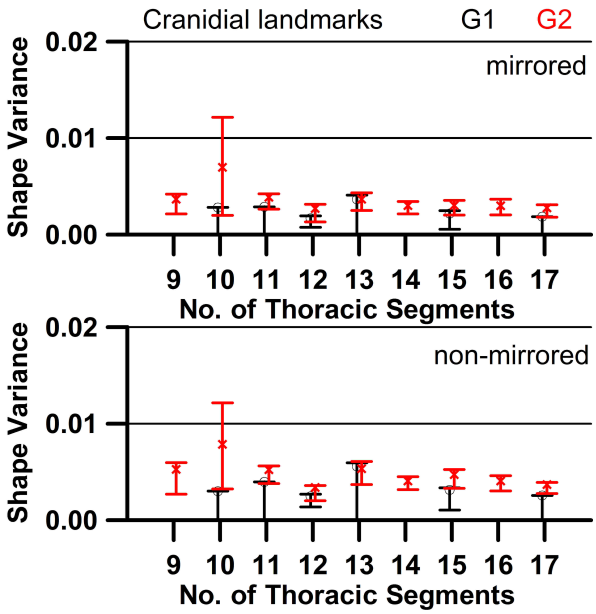

For the mirrored cranidial landmarks, shape variances of G1 and G2 overlap at 95% confidence level at meraspid degree 10, 11, 12, 13 ,15, and 17. For the

non-mirrored data, they are slightly separated at meraspid degree 10 and 17, but amount of separation is minor at about one fifth of the standard error.

Supplementary data 10.

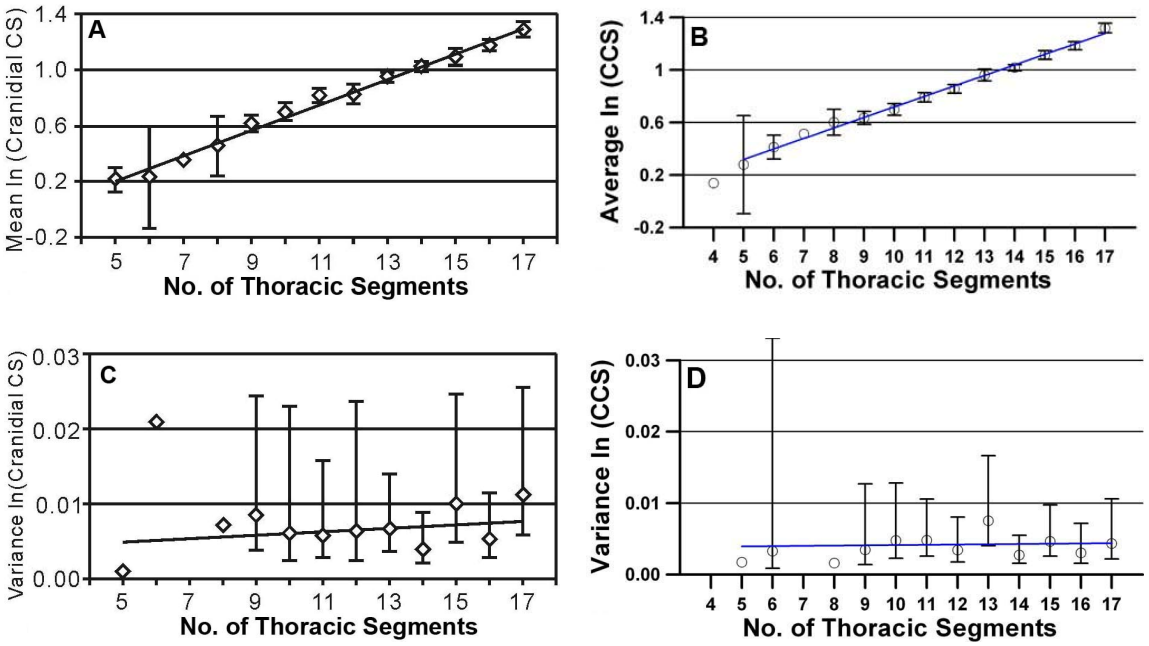

Fusco et al., 2004 New Dataset

Growth (A,B) and variance (C,D) values for cranidial centroid size (CCS) for the previous (A,C) and new (B,D) datasets. The BigFix6 program from the IMP series was used to mirror fifteen landmarks into nine landmarks. Diamonds and circles are the mean logarithm of the CCS for each of the different degrees. Regression lines are shown. Bars in the variance plots are 95% confidence intervals (not calculated for stages with three or less specimens available), method of shortest unbiased confidence intervals (Sokal and Rohlf, 1981).

Supplementary data 11.

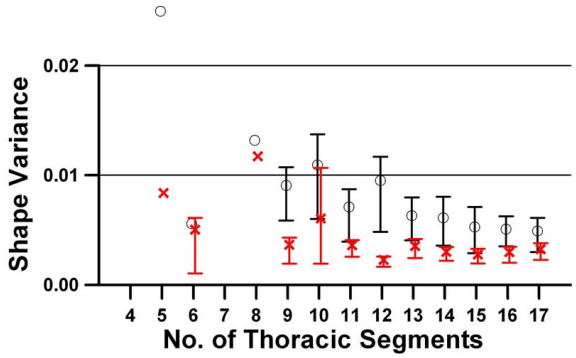

Shape variance values for the cranidium for the previous dataset and the new dataset. Among the 15 landmarks in the cranidium, 6 paired homologous landmarks were reflected across an axial midline for the analysis and averaged, using the program BigFix6 in the morphometrics series IMP. Red x marks are the new materials, and black circles indicate specimens from the previous dataset. Bars are 95% confidence intervals calculated based on 900 bootstrap resamples using DisparityBox6i.

Supplementary data 12.

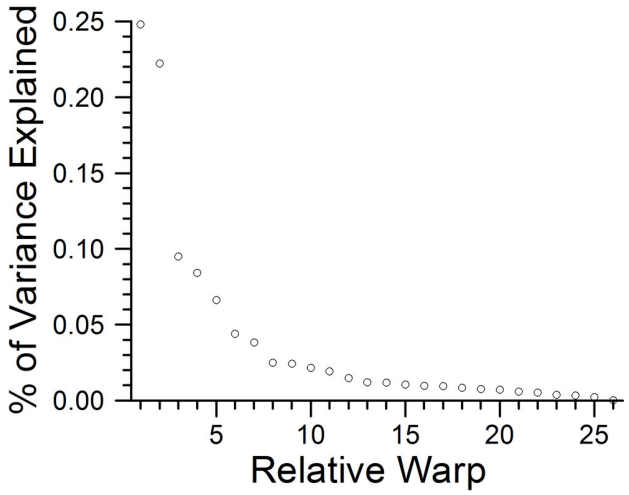

Bivariate plot of percentage of total variance explained by each relative warp of 15 cranidial landmarks for all meraspid and holaspid specimens (N=352). Relative warp (RW) 1 and RW2 each explains 24.80% and 22.23% of total variance.

Supplementary data 13.

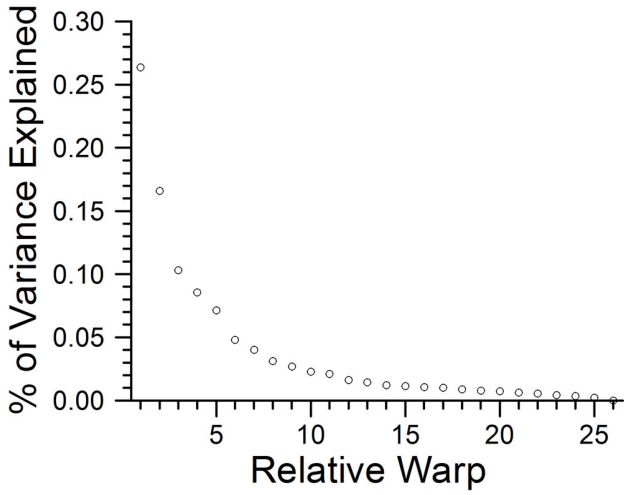

Bivariate plot of percentage of total variance explained by each relative warp of 15 cranidial landmarks of meraspides from meraspid degree 4 through 17 (N=148). Relative warp (RW) 1, RW2, and RW3 each explains 26.35%, 16.58%, and 10.31% of total variance.

Supplementary data 14.

Comparsions of the partial Procrustes distance of cranidial landmarks from the reference specimen (the consensus of the three smallest specimens in the entire dataset) can only be detected when four consecutive meraspid stages are compared – see table below. Results also suggest there is no apparent size-related trend in the degree of morphological difference, as might be expected if the degree of instar-related shape change altered during meraspid ontogeny.

Group1	Group2	n	slope	min	max	p-value
12	15	72	0.0479	0.0096	0.0861	0.0074
13	16	72	0.0498	0.0089	0.0907	0.0088
14	17	69	0.0573	0.0181	0.0965	0.0024
11	15	88	0.0381	0.0098	0.0665	0.0045
12	16	87	0.0521	0.0224	0.0817	0.0004
13	17	86	0.0396	0.0093	0.0817	0.0056
10	15	100	0.0242	0.0001	0.0484	0.0245
11	16	103	0.0432	0.0203	0.0660	0.0001
12	17	101	0.0431	0.0195	0.0667	0.0002
9	15	108	0.0276	0.0066	0.0486	0.0053
10	16	115	0.0310	0.0111	0.0510	0.0013
11	17	117	0.0383	0.0193	0.0572	0.0001
9	16	123	0.0330	0.0154	0.0506	0.0002
10	17	129	0.0300	0.0131	0.0468	0.0003
9	17	137	0.0316	0.0165	0.0467	0.0000

Significant relationships between Partial Procrustes distance with ln CCS among meraspid stages. Only the comparisions that show significant increase in partial Procrustes distance with ln CCS are included in the table. The "Group1" and "Group2" labels are the range of continuous meraspid stages in meraspid degree

numbers. "n" is the sample size, and the "slope" is the regression coefficient of partial Procrustes distance (consensus of smallest three specimens as reference) against ln CCS. The "min" and "max" labels are the lower and upper 95% confidence limits for the slope, and "p-value" is from the significance test of the slope value.

Supplementary data 15.

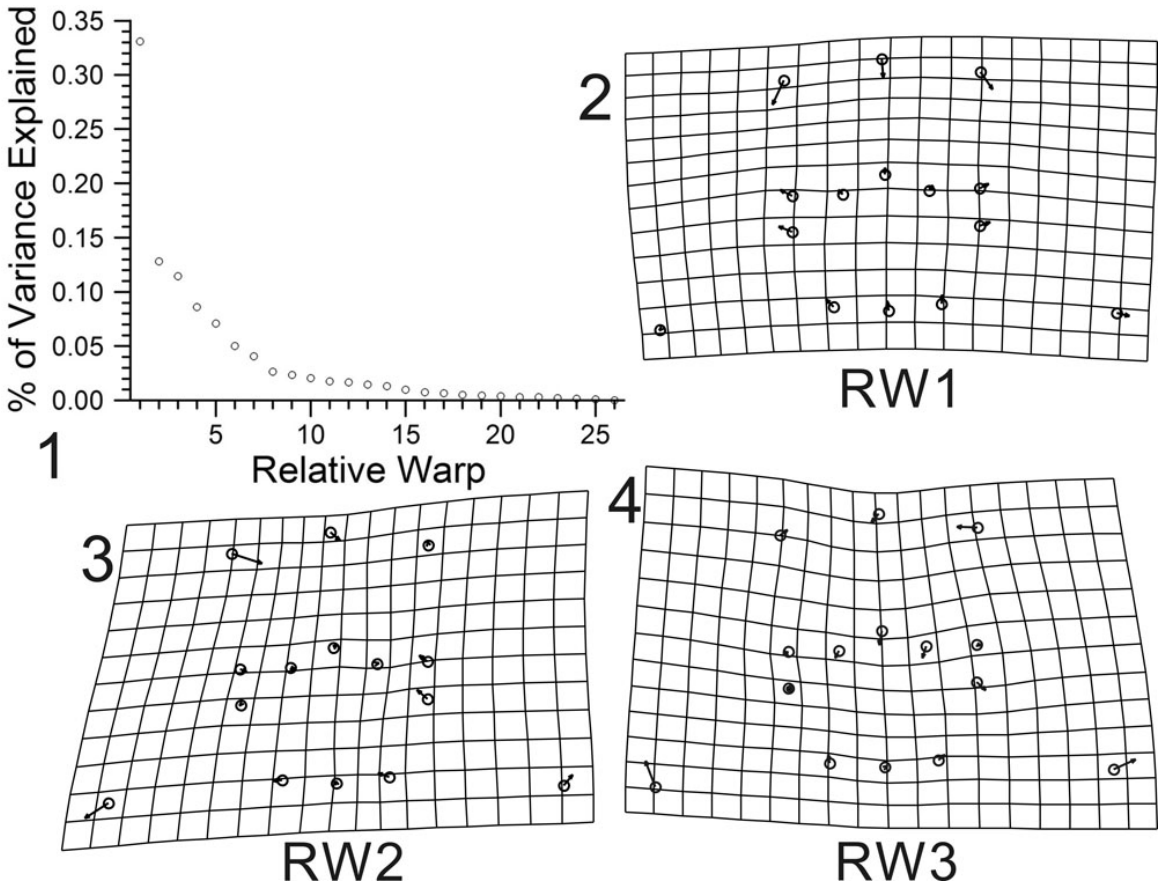

Bivariate plot of percentage of total variance explained by each relative warp of 15 cranidial landmarks for holaspid specimens of 19 morphs with its ln CCS value more than 2.2 (N=54): *1*, Relative warp (RW) 1 explains 33.09% of total variance. Likewise, RW2 12.80%, and RW3 11.45%; *2*, Shape variation related to relative warp 1 (depicting very subtle elongation of the cranidium); *3*, Shape variation related to relative warp 2 (depicting effects of shearing); *4*, Shape

variation related to relative warp 3 (depicting size of the pleural region relative to the glabella and the palpebral lobes).

Supplementary data 16.

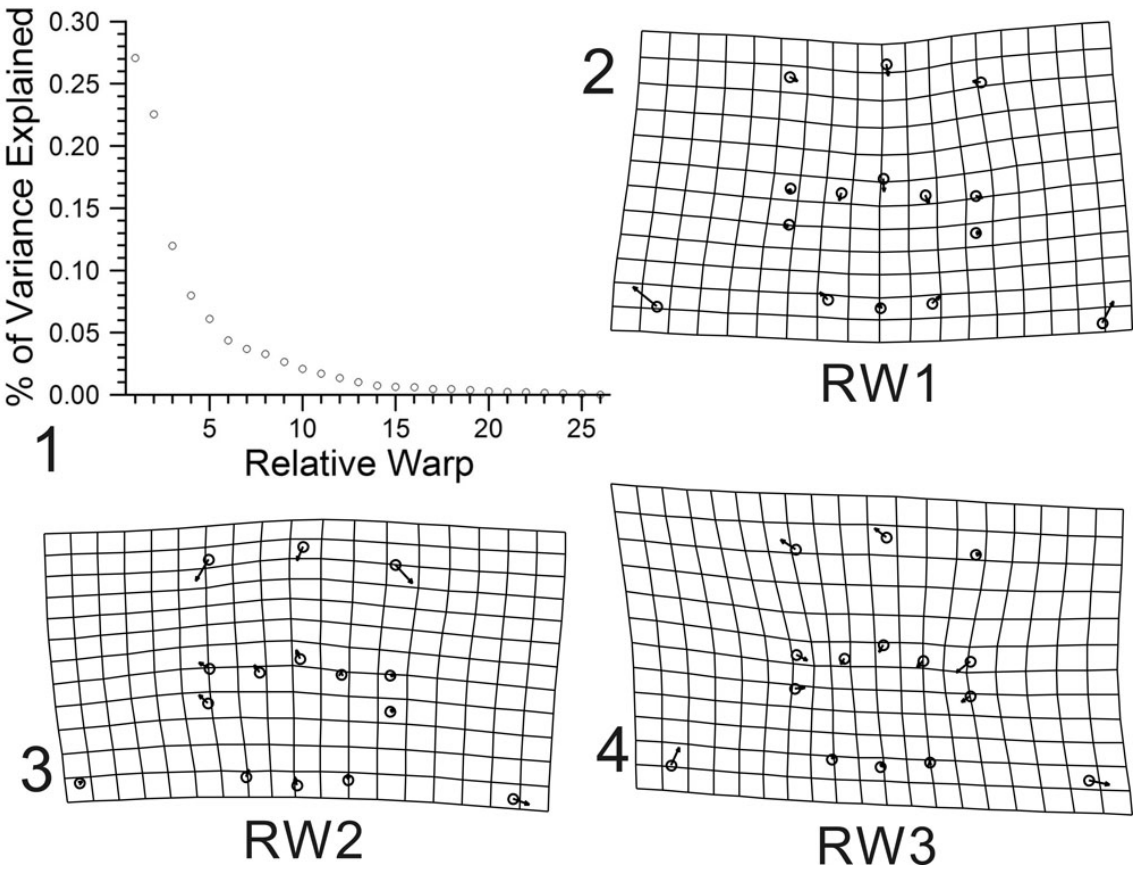

Bivariate plot of percentage of total variance explained by each relative warp of 15 cranidial landmarks for holaspid specimens of 20 morphs with its ln CCS value more than 2.2 (N=42): *1*, Relative warp (RW) 1 explains 27.06% of total variance. Likewise, RW2 22.54%, and RW3 11.97%; *2*, Shape variation related to relative warp 1 (depicting size of the pleural region relative to the glabella and the palpebral lobes); *3*, Shape variation related to relative warp 2 (depicting very

subtle elongation of the cranidium); *4*, Shape variation related to relative warp 3 (depicting effects of shearing).

Supplementary data 17.

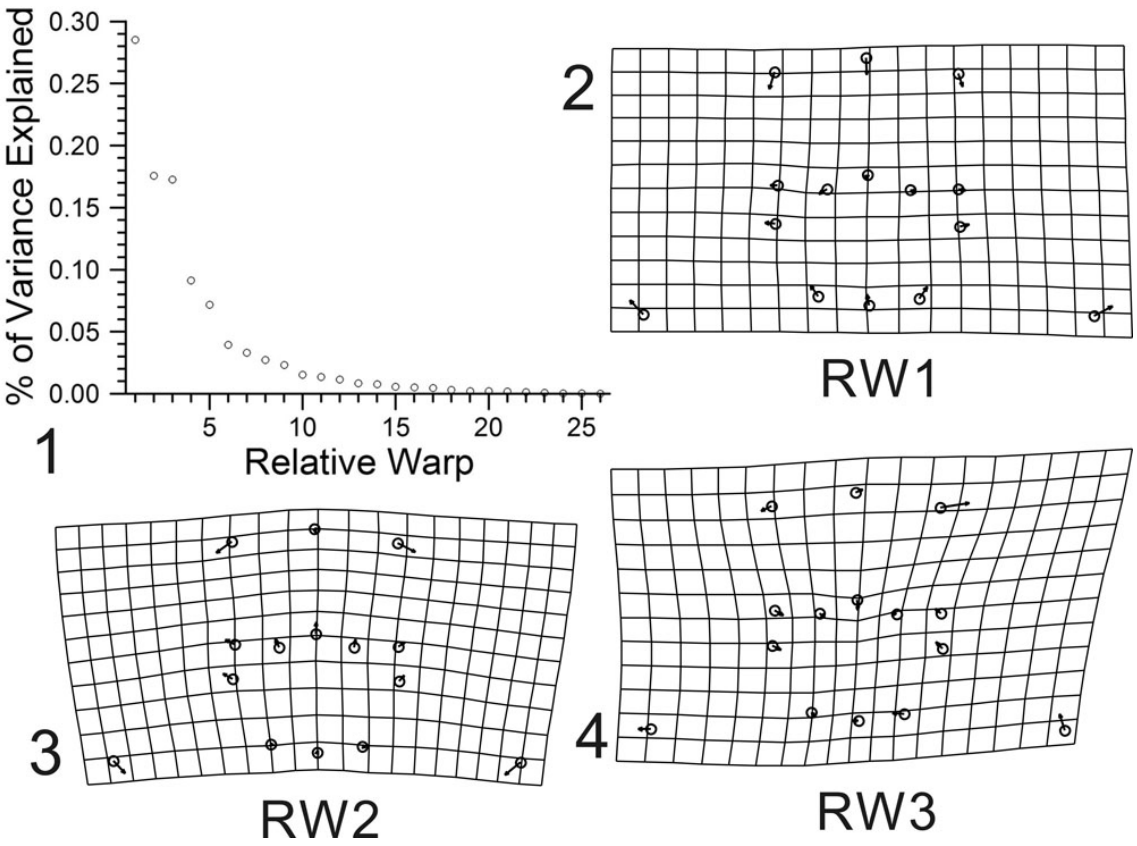

Bivariate plot of percentage of total variance explained by each relative warp of 15 cranidial landmarks for holaspid specimens of 21 morphs with its ln CCS value more than 2.2 (N=30): *1*, Relative warp (RW) 1 explains 28.50% of total variance. Likewise, RW2 17.58%, and RW3 17.27%; *2*, Shape variation related to relative warp 1 (depicting very subtle elongation of the cranidium); *3*, Shape variation related to relative warp 2 (depicting size of the pleural region relative to

the glabella and the palpebral lobes); *4*, Shape variation related to relative warp 3 (depicting effects of shearing).

Supplementary data 18.

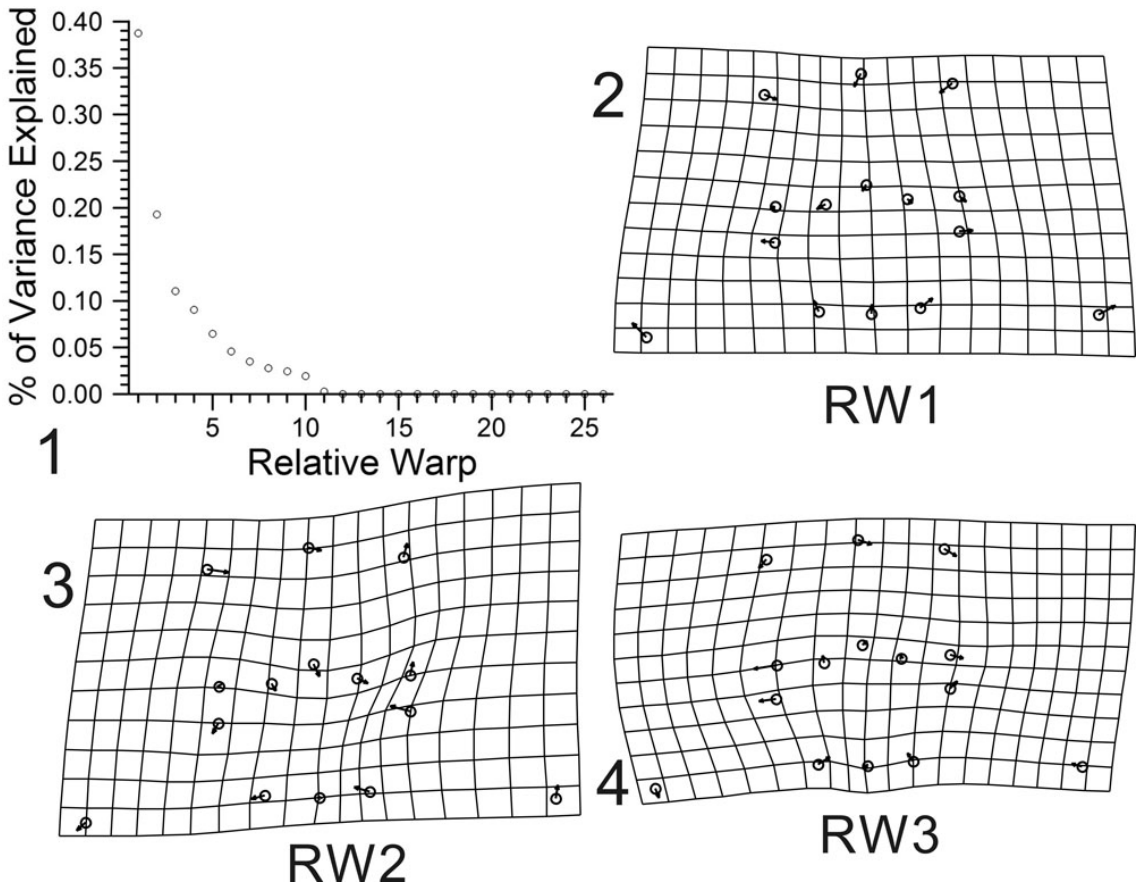

Bivariate plot of percentage of total variance explained by each relative warp of 15 cranidial landmarks for holaspid specimens of 22 morphs with its ln CCS value more than 2.2 (N=12): *1*, Relative warp (RW) 1 explains 38.72% of total variance. Likewise, RW2 19.29%, and RW3 11.04%; *2*, Shape variation related to relative warp 1 (depicting very subtle elongation of the cranidium); *3*, Shape variation related to relative warp 2 (depicting effects of shearing); *4*, Shape

variation related to relative warp 3 (depicting size of the pleural region relative to the glabella and the palpebral lobes).

Supplementary data 19.

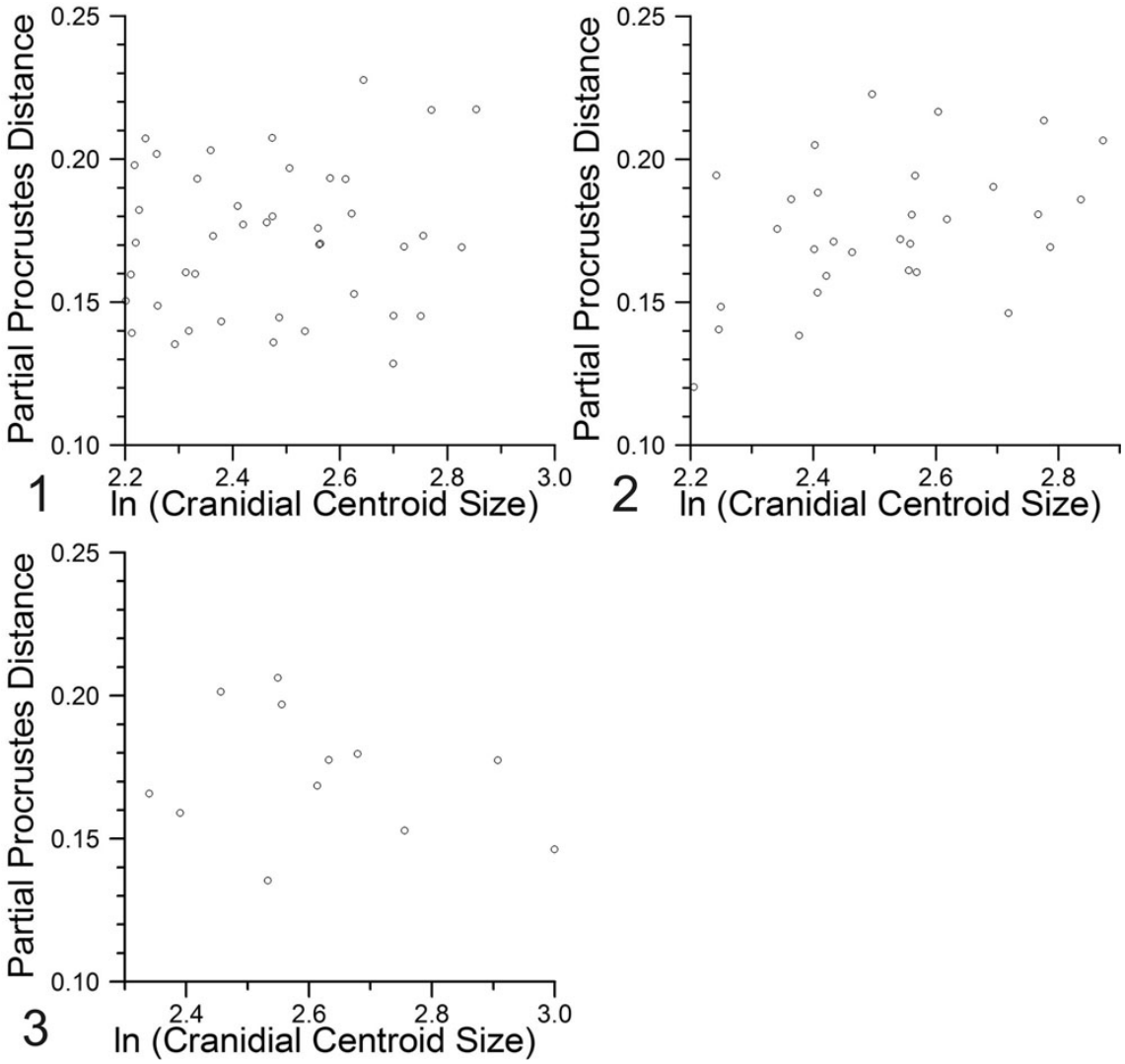

Partial Procrustes distance from the reference (mean shape of the smallest three meraspid specimens) of 15 cranidial landmarks for holaspid specimens of 20 to 22 morphs with its ln CCS value more than 2.2: *1*, 20 morphs (N=42), regression of partial Procrustes distance against logarithm of cranidial centroid size is not

significant at the 95% confidence level (slope=0.0209, P=0.2026, r=0.1325).; *2*, 21 morphs (N=30), regression of partial Procrustes distance against logarithm of cranidial centroid size is significant at the 95% confidence level (slope=0.0566, P=0.008550, r=0.4292); *3*, 22 morphs (N=12), regression of partial Procrustes distance against logarithm of cranidial centroid size is not significant at the 95% confidence level (slope=-0.0263, P=0.7629, r=-0.2341).

Supplementary data 20.

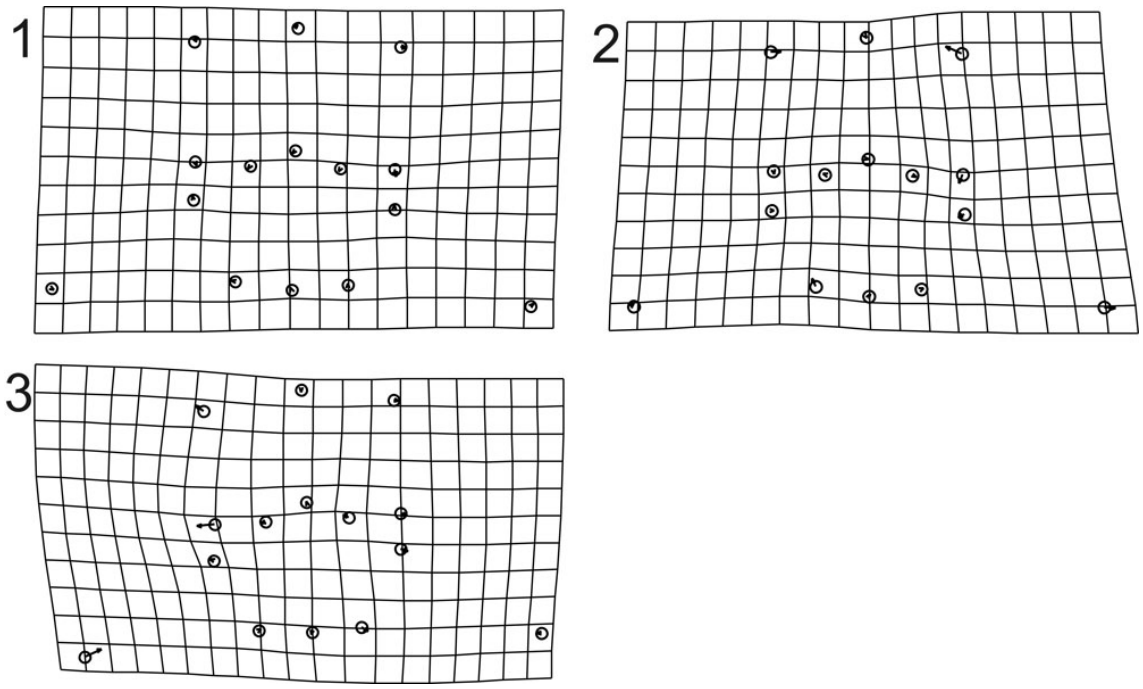

Thin-plate spline deformation grid of shape changes with growth of 15 cranidial landmarks for holaspid specimens of 20 to 22 morphs with its ln CCS value more than 2.2. Partial warp scores are regressed in a multivariate regression against ln centroid size, and percentages are total shape variance (based on summed squared residuals expressed in Procrustes units) explained by the allometry: *1*, 20 morphs (N=42), allometry not significant at the 95% confidence level (1.82% of total variance explained, p=0. 6525 from 1600 bootstraps); *2*, 21 morphs (N=30), allometry not significant at the 95% confidence level (4.49% of total variance explained, p=0. 2175 from 1600 bootstraps); *3*, 22 morphs (N=12),

allometry not significant at the 95% confidence level (7.50% of total variance explained, p=0.56625 from 1600 bootstraps).

Supplementary data 21.

The vectors of regression coefficients (calculated from regressing partial warp scores in a multivariate regression against ln CCS; mean shape is used as a reference for the partial warp scores) for the 15 cranidial landmarks of holaspid specimens of 19 to 22 morphs are compared with isometry. Angle of the normalized vector within the sample and angle to isometry is compared at the 95% confidence level by 1600 bootstraps.

Holaspides (ln CCS > 2.2)	N	angle to isometry	within sample	Significant difference
19 morphs	54	101.5°	86.3°	yes
20 morphs	42	115.7°	87.4°	yes
21 morphs	30	81.1°	77.0°	yes
22 morphs	12	87.2°	91.7°	no

Supplementary data 22.

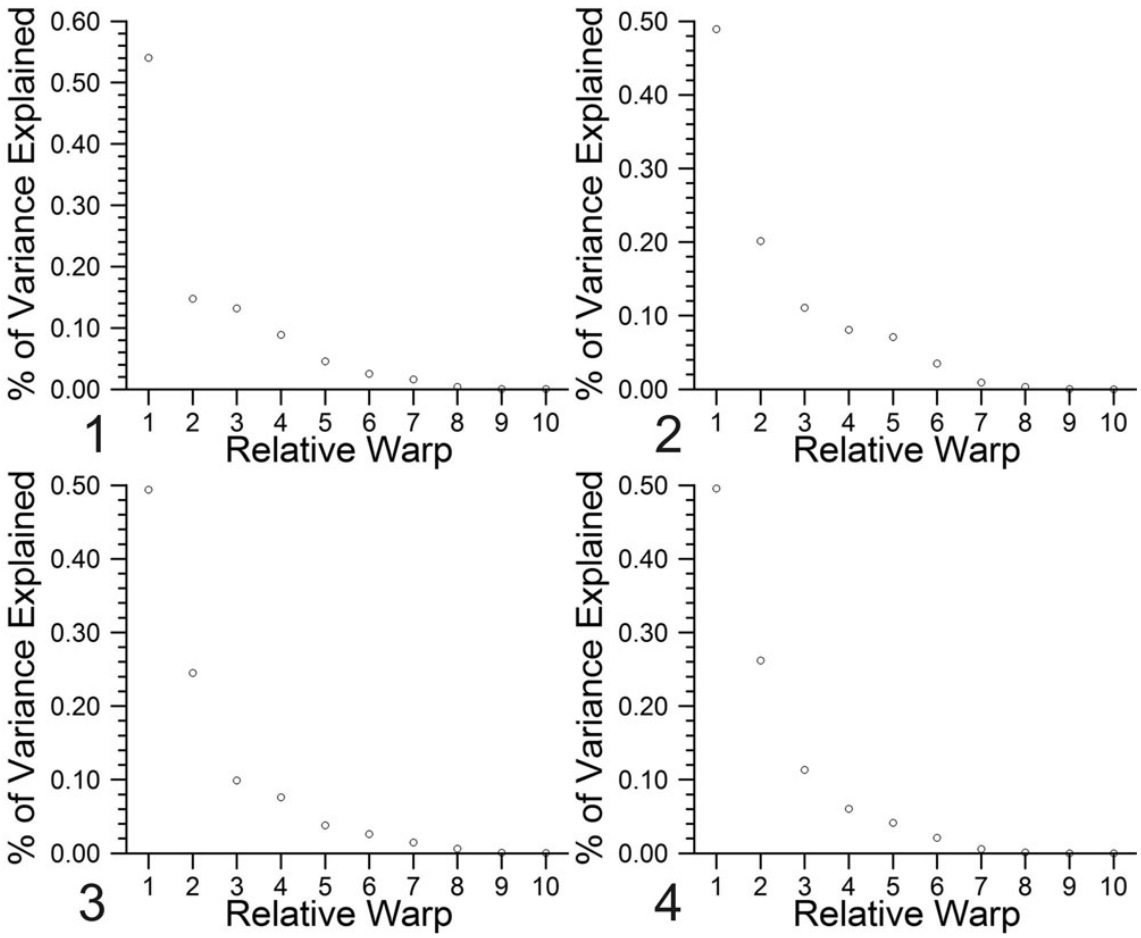

Bivariate plot of percentage of total variance explained by each relative warp of 7 pygidial landmarks for specimens of 19 to 22 morphs with its ln cranidial centroid size value being over 2.2. Percentage of total shape variance (based on summed squared residuals expressed in Procrustes units) explained by the allometry in parentheses: *1*, 19 morphs (N=54), Relative Warp (RW) 1 (54.03%), RW2 (14.78%), RW3 (13.19%); *2*, 20 morphs (N=42), RW1 (48.92%), RW2 (20.12%),

RW3 (11.08%); *3*, 21 morphs (N=30), RW1 (49.38%), RW2 (24.51%), RW3 (9.90%); *4*, 22 morphs (N=12), RW1 (49.58%), RW2 (26.19%), RW3 (11.32%).

Supplementary data 23.

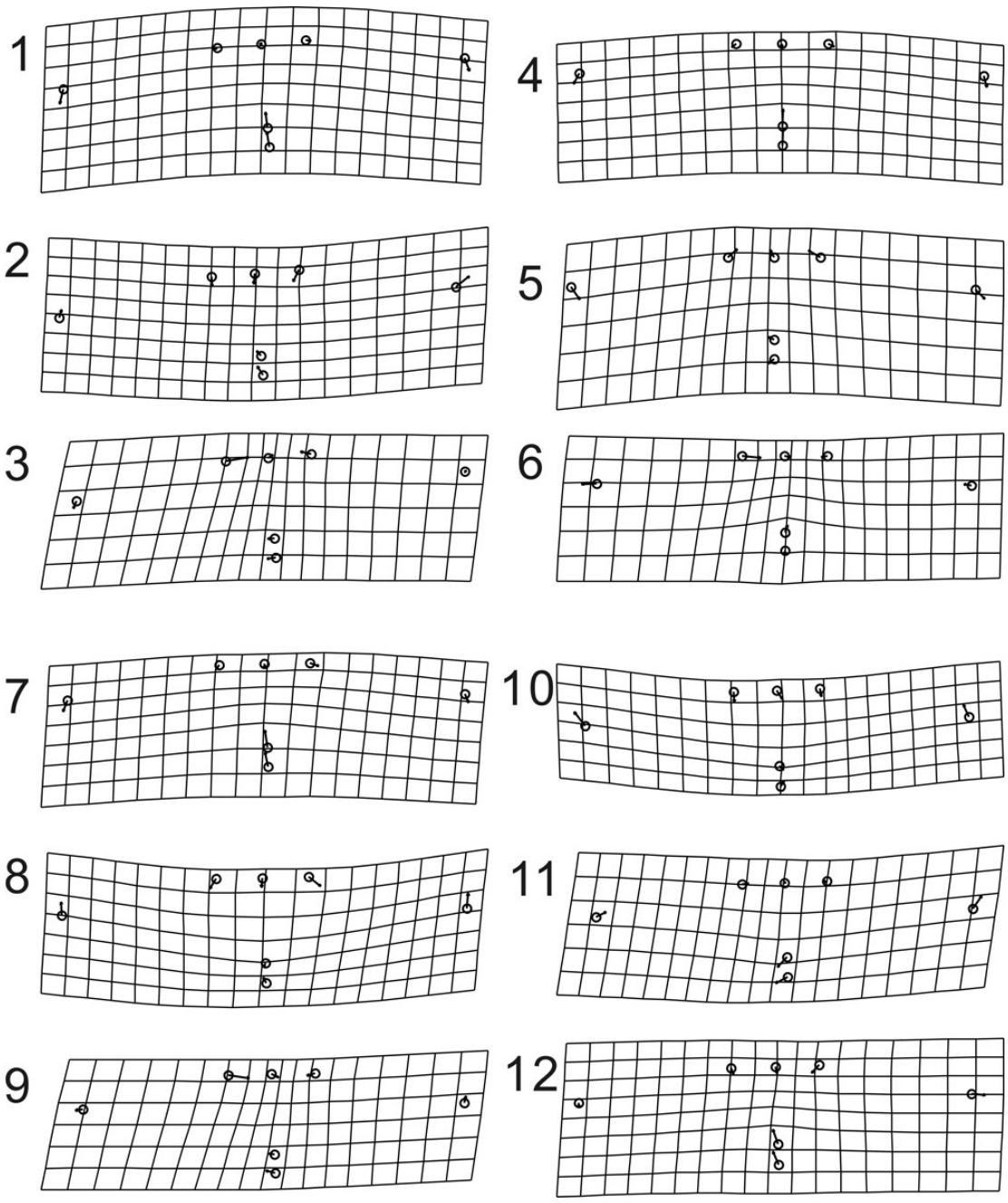

Bivariate plot of percentage of total variance explained by each relative warp of 15 cranidial landmarks for holaspid specimens of 19 to 22 morphs with its ln CCS value more than 2.2. Partial warp scores are regressed in a multivariate regression against ln pygidial centroid size, and percentage of total shape variance (based on summed squared residuals expressed in Procrustes units) explained by the allometry in parentheses: *1*–*3*, 19 morphs (N=54); *1*, Relative Warp (RW) 1 (54.03%); *2*, RW2 (14.78%); *3*, RW3 (13.19%); *4*–*6*, 20 morphs (N=42); *4*, RW1 (48.92%); *5*, RW2 (20.12%); *6*, RW3 (11.08%); *7*–*9*, 21 morphs (N=30); *7*, RW1 (49.38%); *8*, RW2 (24.51%); *9*, RW3 (9.90%); *10*–*12*, 22 morphs (N=12); *10*, RW1 (49.58%); *11*, RW2 (26.19%); *12*, RW3 (11.32%); *1*, *4*, *7*, *10*, Shape changes related to RW1 is arching of the whole pygidium and variations in the axis-direction distance between mid-posterior end of the pygidium and the anterolateral tips of the pygidium; *2*, *5*, *8*, *11*, RW2 represents variations in the relative length of the pygidium; *3*, *6*, *9*, *12*, RW3 represents variations in the width of the pygidial axis.

Supplementary data 24.

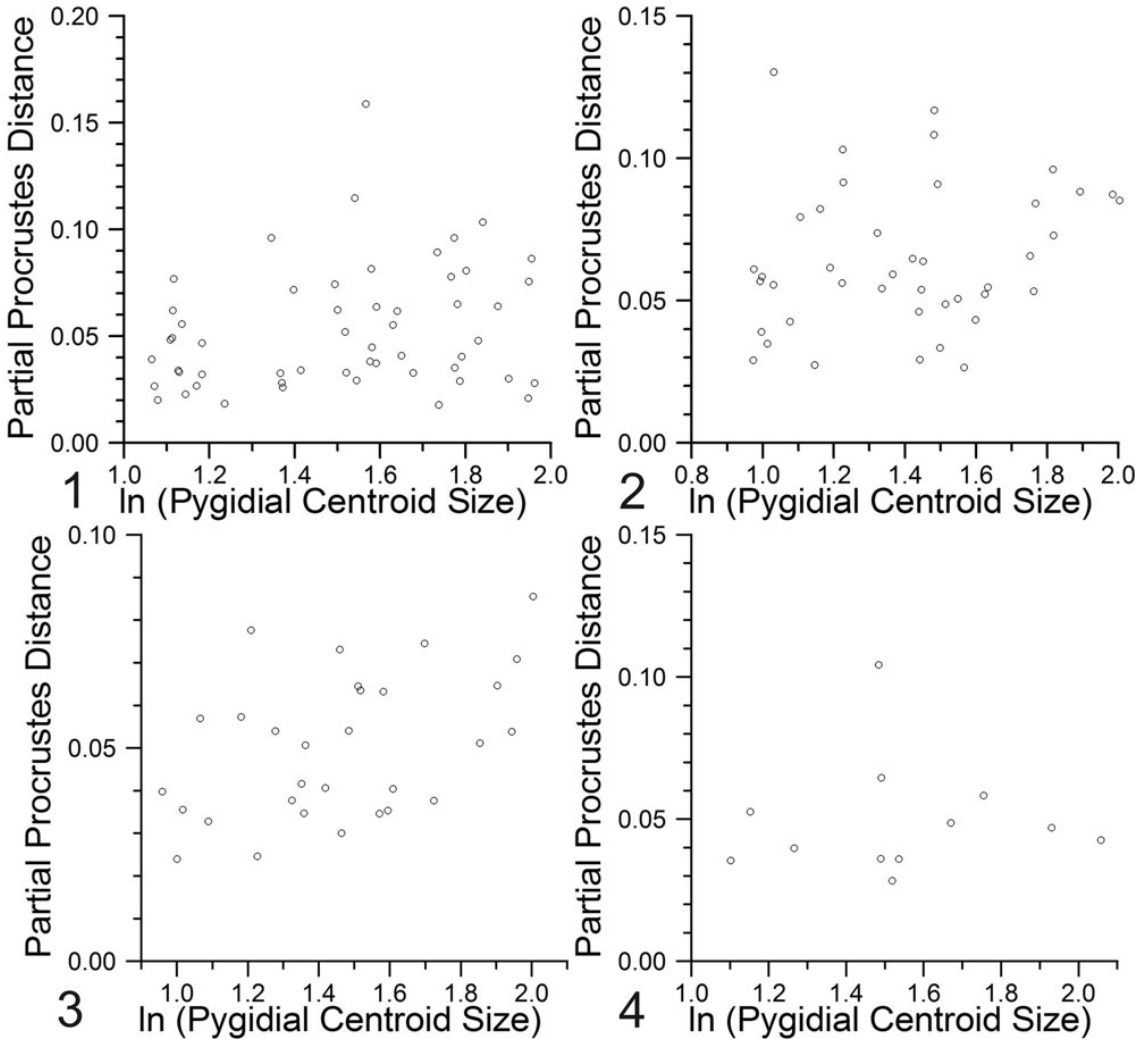

Partial Procrustes distance from the reference (mean shape of the smallest three specimens in each holaspid sample) of 7 pygidial landmarks for holaspid specimens of 19 to 22 morphs with its ln CCS value more than 2.2. Regression of partial Procrustes distance against logarithm of pygidial centroid size is significant for 19 and 21 morphs. *1*, 19 morphs (slope=0.0241, P=0.0395,

r=0.2412, N=54); *2*, 20 morphs (slope=0.0176, P=0.09248, r=0.2091, N=42); *3*, 21 morphs (slope=0.0262, P=0.0044, r=0.4649, N=30); *4*, 22 morphs (slope=0.0025, P=0.4577, r=0.0354, N=12).

Supplementary data 25.

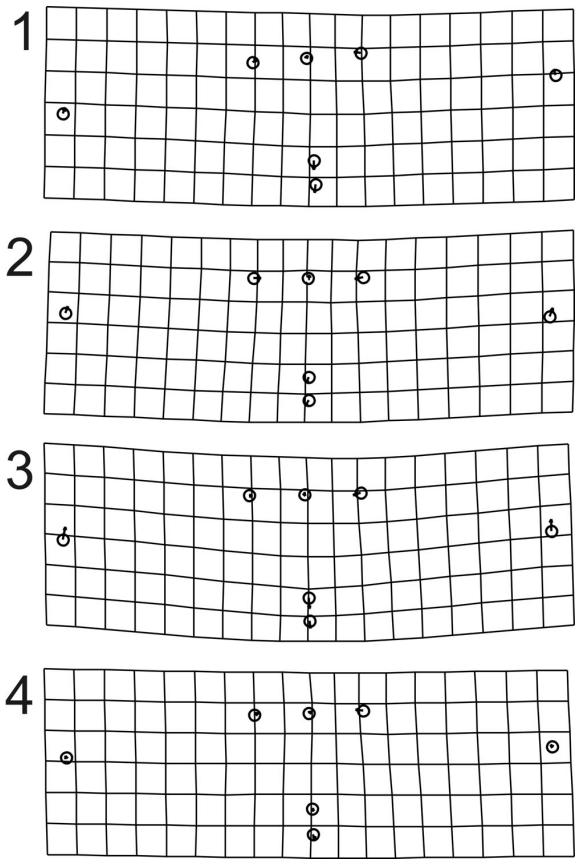

Thin-plate spline deformation grid of shape changes with growth of 7 pygidial landmarks for holaspid specimens of 19 to 22 morphs with its ln CCS value more than 2.2. Partial warp scores are regressed in a multivariate regression against ln pygidial centroid size. *1*, 19 morph, 9.40% of total shape variance (based on summed squared residuals expressed in Procrustes units) is explained by the allometry (P=0.001875 from 1600 bootstraps); *2*, 20 morph, 8.86% of total shape variance (based on summed squared residuals expressed in Procrustes units) is

explained by the allometry (P=0.0075 from 1600 bootstraps); *3*, 21 morph, 15.32% of total shape variance is explained by the allometry (P=0.003750 from 1600 bootstraps); *4*, 22 morph, 3.47% of total shape variance is explained by the allometry (P=0.08675 from 1600 bootstraps).

Supplementary data 26.

The vectors of regression coefficients (calculated from regressing partial warp scores in a multivariate regression against ln CCS; mean shape is used as a reference for the partial warp scores) for the 7 pygidial landmarks of holaspid specimens of 19 to 22 morphs are compared with isometry. Angle of the normalized vector within the sample and angle to isometry is compared at the 95% confidence level by 1600 bootstraps.

Holaspides (ln CCS > 2.2)	N	angle to isometry	within sample	Significant difference
19 morphs	54	99.1°	46.7°	yes
20 morphs	42	103.5°	56.7°	yes
21 morphs	30	81.9°	49.6°	yes
22 morphs	12	97.9°	111.3°	no

Supplementary data 27.

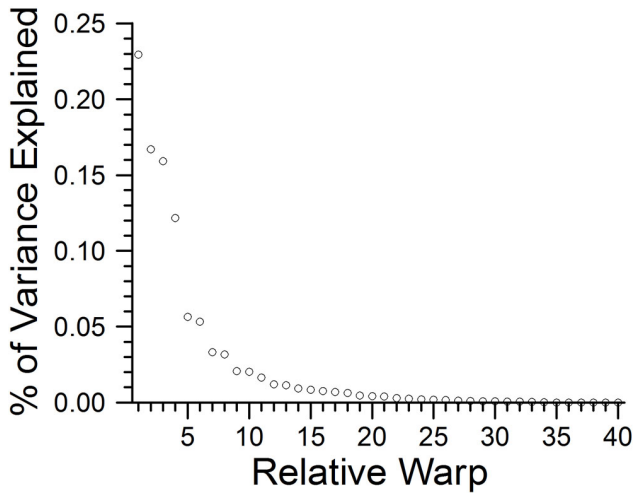

Bivariate plot of percentage of total variance explained by each relative warp of 22 exoskeletal landmarks for specimens of 19 morphs with its ln cranidial centroid size value being over 2.2 (N=54). Relative warp (RW) 1 explains 22.94% of total variance. Likewise, RW2 16.71%, RW3 15.90%, and RW4 12.16%.

Supplementary data 28.

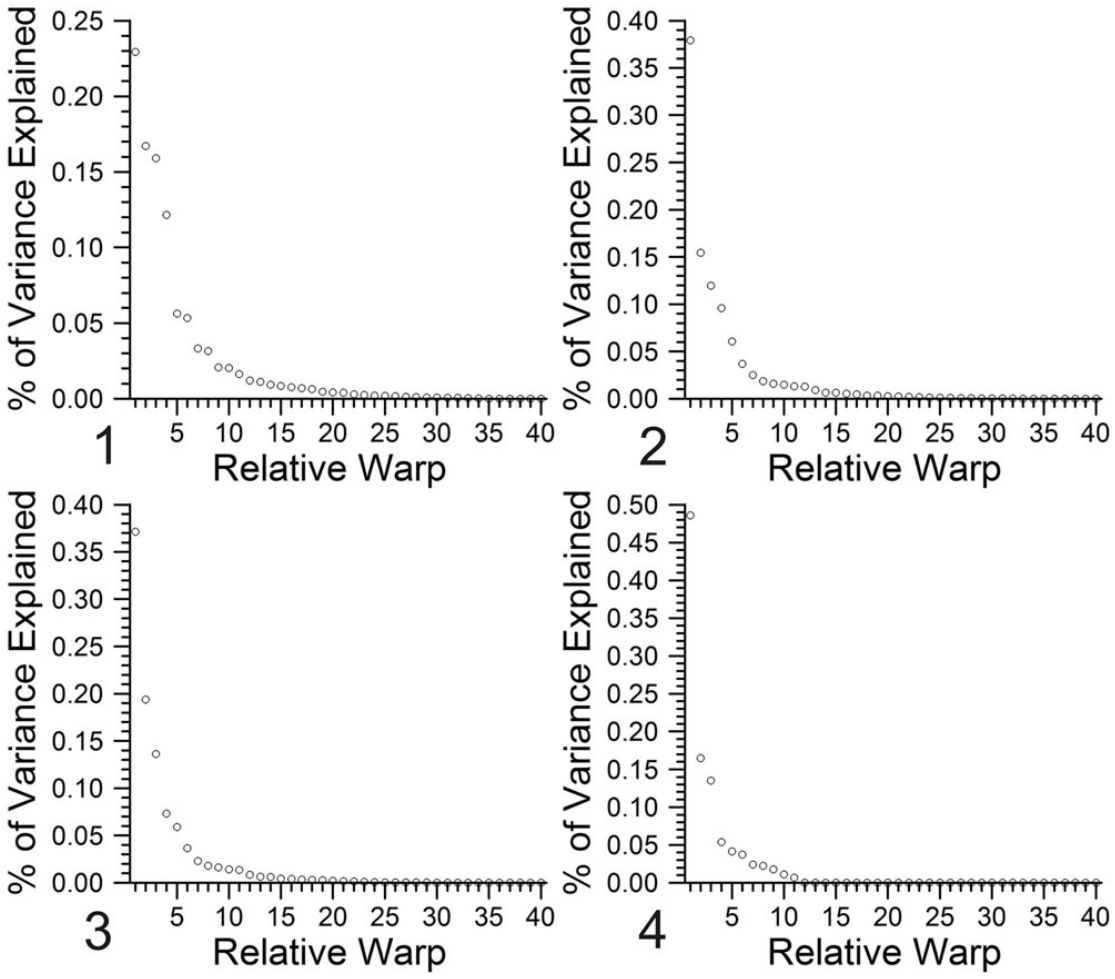

Bivariate plot of percentage of total variance explained by each relative warp of 22 exoskeletal landmarks for specimens of 19 to 22 morphs with its ln cranidial centroid size value being over 2.2. Percentage of total shape variance (based on summed squared residuals expressed in Procrustes units) explained by the allometry in parentheses: *1*, 19 morphs (N=54), Relative Warp (RW) 1 (22.94%), RW2 (16.71%), RW3 (15.90%), RW4 (12.16%); *2*, 20 morphs (N=42), RW1

(37.93%), RW2 (15.45%), RW3 (11.96%), RW4 (9.60%); *3*, 21 morphs (N=30), RW1 (37.14%), RW2 (19.38%), RW3 (13.61%), RW4 (7.31%); *4*, 22 morphs (N=12), RW1 (48.57%), RW2 (16.47%), RW3 (13.51%), RW4 (5.37%).

Supplementary data 29.

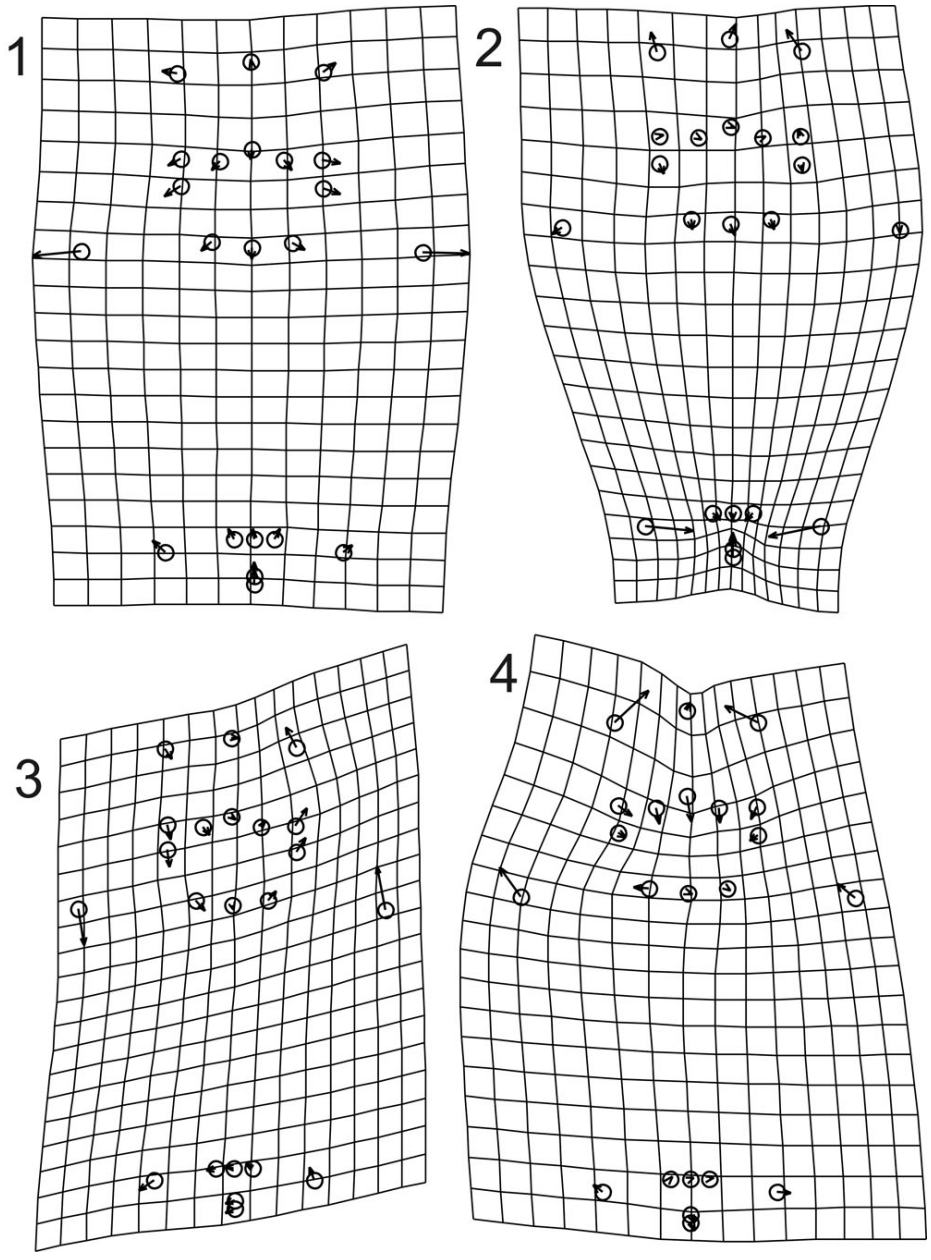

Thin-plate spline deformation grid of relative warps of 22 exoskeletal landmarks for holaspid specimens of 20 morphs with its ln CCS value more than 2.2 (N=42):

1, Shape variation related to relative warp 1 (37.93% of total variance explained);

2, Shape variation related to relative warp 2 (15.45% of total variance explained);

3, Shape variation related to relative warp 3 (11.96% of total variance explained);

4, Shape variation related to relative warp 4 (9.60% of total variance explained).

Supplementary data 30.

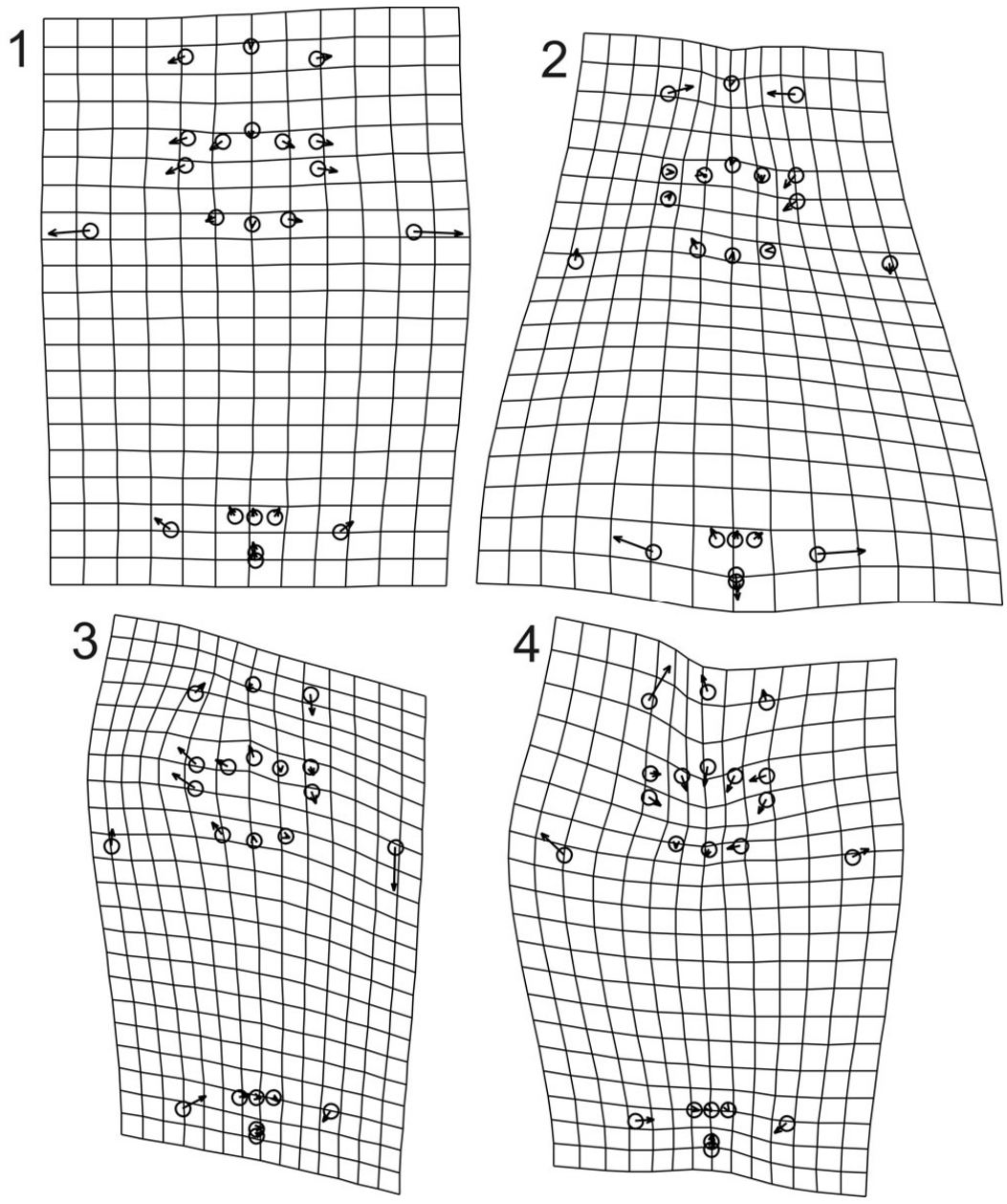

Thin-plate spline deformation grid of relative warps of 22 exoskeletal landmarks for holaspid specimens of 21 morphs with its ln CCS value more than 2.2 (N=30):

1, Shape variation related to relative warp 1 (37.14% of total variance explained);

2, Shape variation related to relative warp 2 (19.38% of total variance explained);

3, Shape variation related to relative warp 3 (13.61% of total variance explained);

4, Shape variation related to relative warp 4 (7.31% of total variance explained).

Supplementary data 31.

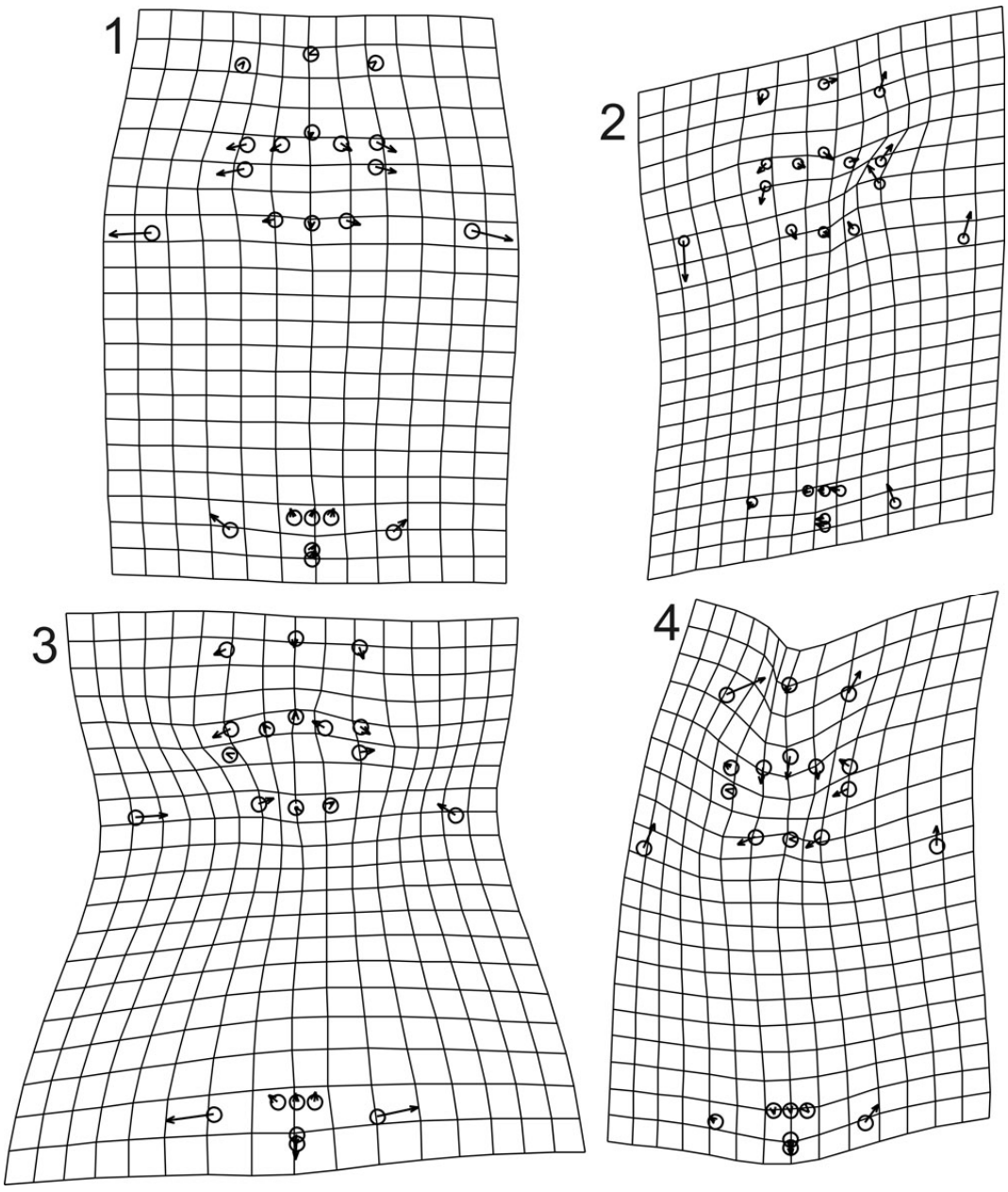

Thin-plate spline deformation grid of relative warps of 22 exoskeletal landmarks for holaspid specimens of 22 morphs with its ln CCS value more than 2.2 (N=12):

1, Shape variation related to relative warp 1 (48.57% of total variance explained);

2, Shape variation related to relative warp 2 (16.47% of total variance explained);

3, Shape variation related to relative warp 3 (13.51% of total variance explained);

4, Shape variation related to relative warp 4 (5.37% of total variance explained).

Supplementary data 32.

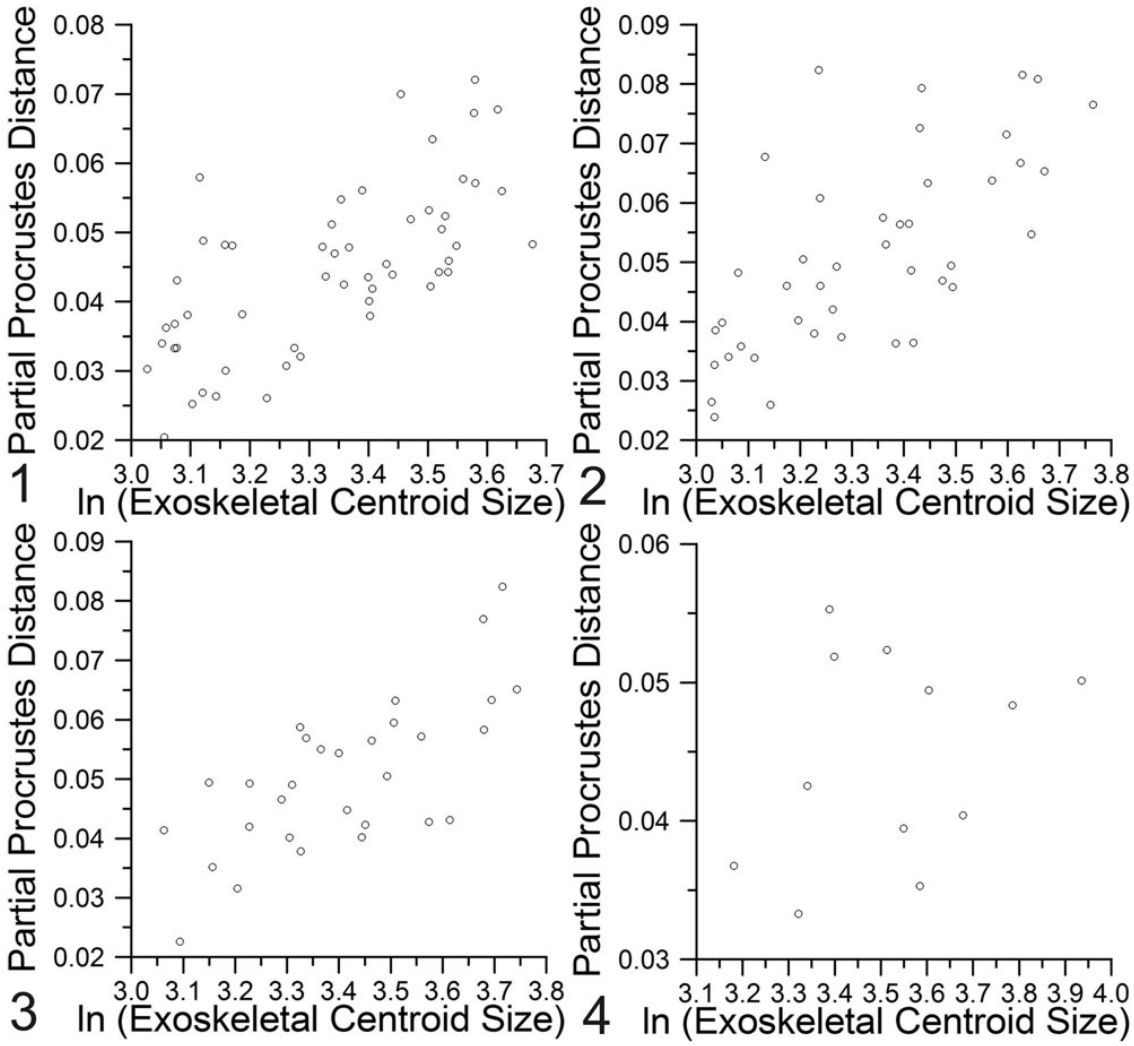

Partial Procrustes distance from the reference (mean shape of the smallest three specimens in each holaspid sample) of 22 exoskeletal landmarks for holaspid specimens of 19 to 22 morphs with its ln CCS value more than 2.2. Regression of partial Procrustes distance against logarithm of exoskeletal centroid size is significant for 19 to 21 morphs and it is not significant for the 22 morph. *1*, 19

morphs (slope=0.0425, P<0.0001, r=0.6792, N=54); *2*, 20 morphs (slope=0.0533, P<0.0001, r=0.6861, N=42); *3*, 21 morphs (slope=0.0473, P<0.0001, r=0.7085, N=30); *4*, 22 morphs (slope=0.0105, P=0.1786, r=0.2977, N=12).

Supplementary data 33.

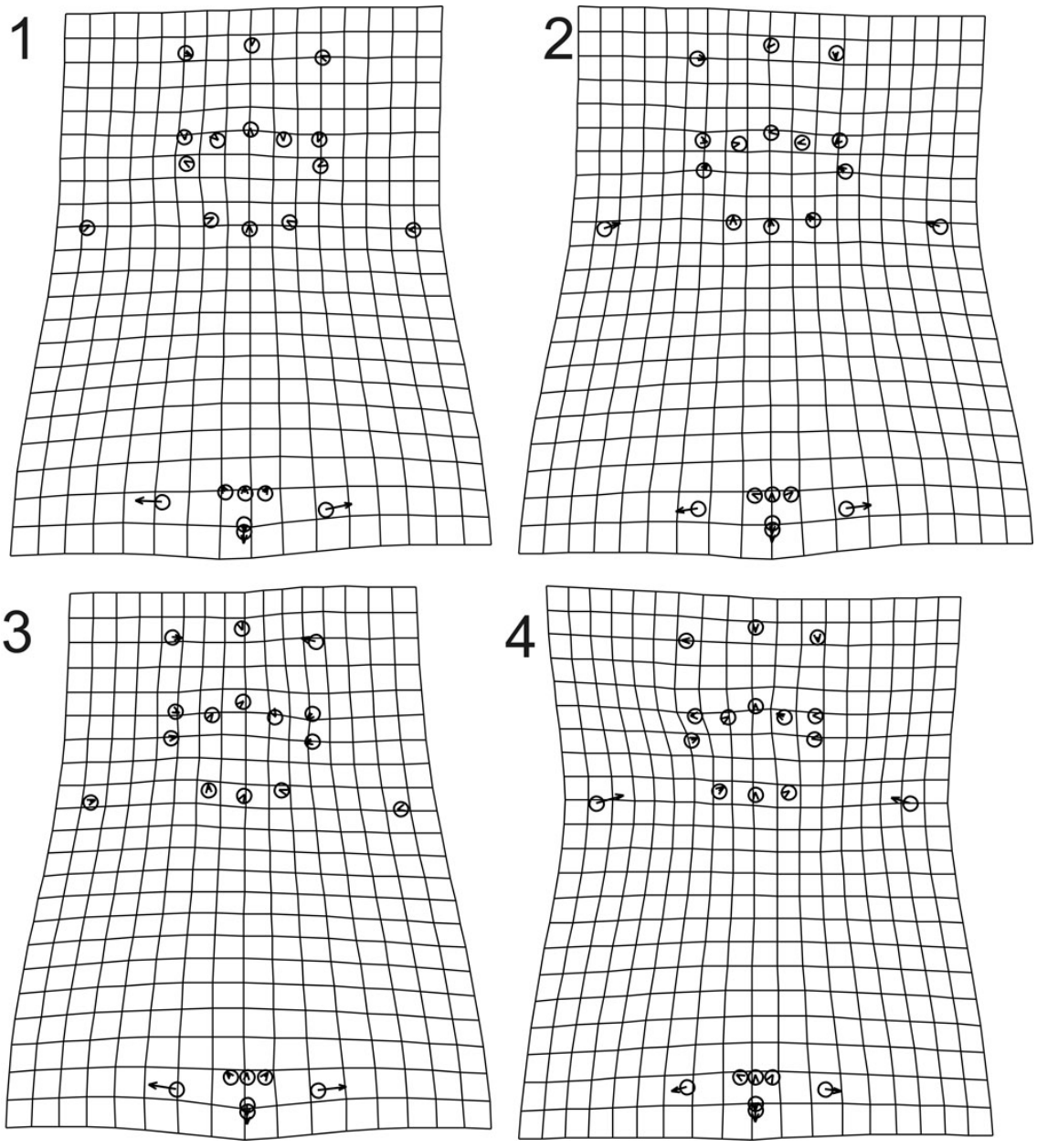

Thin-plate spline deformation grid of shape changes with growth of 22 exoskeletal landmarks for holaspid specimens of 19 to 22 morphs with its ln CCS

value more than 2.2. Partial warp scores are regressed in a multivariate regression against ln exoskeletal centroid size. *1*, 19 morph, 14.79% of total shape variance (based on summed squared residuals expressed in Procrustes units) is explained by the allometry (P<0.000625 from 1600 bootstraps); *2*, 20 morph, 13.50% of total shape variance (based on summed squared residuals expressed in Procrustes units) is explained by the allometry (P<0.000625 from 1600 bootstraps); *3*, 21 morph, 15.46% of total shape variance is explained by the allometry (P<0.000625 from 1600 bootstraps); *4*, 22 morph, 13.50% of total shape variance is explained by the allometry (P=0.17 from 1600 bootstraps).

Supplementary data 34.

The vectors of regression coefficients (calculated from regressing partial warp scores in a multivariate regression against ln CCS; mean shape is used as a reference for the partial warp scores) for the 22 exoskeletal landmarks of holaspid specimens of 19 to 22 morphs are compared with isometry. Angle of the normalized vector within the sample and angle to isometry is compared at the 95% confidence level by 1600 bootstraps.

Holaspides (ln CCS > 2.2)	N	angle to isometry	within sample	Significant difference
19 morphs	54	74.5°	35.2°	yes
20 morphs	42	83.8°	45.0°	yes
21 morphs	30	85.9°	49.4°	yes
22 morphs	12	91.1°	78.8°	yes